





UNO: Unlimited Sampling Meets One-Bit Quantization

Arian Eamaz , Graduate Student Member, IEEE, Kumar Vijay Mishra , Senior Member, IEEE, Farhang Yeganegi , and Mojtaba Soltanalian , Senior Member, IEEE

Abstract—Recent results in one-bit sampling provide a framework for a relatively low-cost, low-power sampling, at a high rate by employing time-varying sampling threshold sequences. Another recent development in sampling theory is unlimited sampling, which is a high-resolution technique that relies on *modulo ADCs* to yield an unlimited dynamic range. In this paper, we leverage the appealing attributes of the two aforementioned techniques to propose a novel *unlimited one-bit (UNO) sampling approach*. In this framework, the information on the distance between the input signal value and the threshold is stored and utilized to accurately reconstruct the one-bit sampled signal. We then utilize this information to accurately reconstruct the signal from its one-bit samples via the randomized Kaczmarz algorithm (RKA). In the presence of noise, we employ the recent plug-and-play (PnP) priors technique with alternating direction method of multipliers (ADMM) to exploit integration of state-of-the-art regularizers in the reconstruction process. Numerical experiments with RKA and PnP-ADMM-based reconstruction illustrate the effectiveness of our proposed UNO, including its superior performance compared to the one-bit $\Sigma\Delta$ sampling.

Index Terms—Kaczmarz algorithm, one-bit quantization, PnP-ADMM, modulo ADCs, unlimited sampling.

I. INTRODUCTION

SAMPLING theory lies at the heart of all modern digital processing systems. A seminal result in this context, referred to as Whittaker-Kotelnikov-Shannon (or, simply Shannon's) theorem, states that it is possible to fully recover a bandlimited function from values measured on a regular sampling grid as long as the function's support is an interval with length not exceeding the density of the sampling grid. Restating this in signal processing terms, a lowpass bandlimited signal can be perfectly reconstructed from its discrete samples taken uniformly at a

Manuscript received 10 December 2022; revised 27 June 2023 and 16 November 2023; accepted 16 January 2024. Date of publication 25 January 2024; date of current version 20 February 2024. This work was supported in part by the National Science Foundation under Grant CCF-1704401. An earlier version of this paper was presented at the 2023 IEEE International Conference on Sampling Theory and Applications (SampTA) [DOI: 10.1109/SampTA59647.2023.10301408]. The associate editor coordinating the review of this manuscript and approving it for publication was Prof. Laurent Jacques. (Corresponding author: Arian Eamaz.)

Arian Eamaz, Farhang Yeganegi, and Mojtaba Soltanalian are with the Department of Electrical and Computer Engineering, University of Illinois Chicago, Chicago, IL 60607 USA (e-mail: aeamaz2@uic.edu; fyegan2@uic.edu; msol@uic.edu).

Kumar Vijay Mishra is with the United States DEVCOM Army Research Laboratory, Adelphi, MD 20783 USA (e-mail: kvm@ieee.org).

Digital Object Identifier 10.1109/TSP.2024.3356253

sampling frequency that is at least the Nyquist rate, i.e., twice the signal bandwidth [1].

Shannon's theorem assumes the existence of samples that are of infinite precision and infinite dynamic range (DR). But, in practice, it is realized by the quantization of the signals through analog-to-digital converters (ADCs) that clip or saturate whenever the signal amplitude exceeds the maximum recordable ADC voltage, leading to a permanent information loss. There is a long legacy of literature on clipping [2], [3], [4], especially for audio [5] and communications [2] signals. In particular, [2] investigated the effects of noise when it is passed through both linear and nonlinear devices, such as a clipper. Substantial work has been done and is still ongoing to overcome this problem, and the literature is too large to summarize here; see, e.g., [6] and the references therein, for comparisons of various techniques. Overall, these approaches require declipping [7], multiple ADCs [8], and scaling techniques [9], which are expensive and cumbersome. Recently, some studies [6], [10], [11], [12] have proposed the *unlimited sampling* or modulo sampling architecture to fully overcome this limitation by employing modular arithmetic. The term "unlimited sampling" stems from the sampling theorem outlined in [6], [10], wherein the sampling rate of the proposed scheme is independent of the ratio between the input signal DR and the ADC threshold. To perfectly reconstruct the signal of interest from modulo samples (up to an unknown constant), the unlimited sampling theory suggests the sampling rate to be slightly higher than the Nyquist rate and the upper bound of the infinity norm of the bandlimited signal be known.

Conventional multi-bit ADCs require a very large number of quantization levels to represent the original continuous signal in high resolution settings. Sampling at high data rates with high resolution ADCs, however, would dramatically increase the overall power consumption and the manufacturing cost of such ADCs [13]. This problem is exacerbated in systems that require multiple ADCs such as large array receivers [14]. An immediate solution to such challenges is to use fewer bits for sampling. Therefore, in the recent years, the design of receivers with low-complexity *one-bit ADC* has been emphasized to meet the requirements of both wide signal bandwidth and low cost/power. *One-bit quantization* is an extreme quantization scenario, in which the ADCs are merely comparing the signals with given threshold levels, producing sign (± 1) outputs. This enables the signal processing equipment to sample at a very high rate yet with considerably lower cost and energy

consumption than the conventional ADCs [15], [16], [17], [18]. Several applications abound of one-bit ADCs, such as multiple-input multiple-output wireless communications [16], [19], channel estimation [20], and array signal processing [21]. These were preceded by one-bit $\Sigma\Delta$ techniques [22], [23]. In this paper, we focus on the *memoryless scalar quantization* which unlike the $\Sigma\Delta$ quantization, does not need any feedback or update process.

In the classical problem of one-bit quantization, the signal is reconstructed by comparing the signal with a fixed, usually zero, threshold. This leads to difficulties in estimating signal parameters. In particular, when zero threshold is used, the power information of the input signal \mathbf{x} is lost in one-bit data because the signs of \mathbf{x} and $\eta\mathbf{x}$ are identical for $\eta > 0$. This problem has been addressed in a few recent works [17], [24], [25], [26], [27], [28], [29], [30], which show that time-varying sampling thresholds enable better estimation of the signal characteristics. The time-varying thresholds are realized through a randomly (usually, Gaussian and Uniform) dithered generator within the ADC [31]. The source of this Gaussian dither is a low-cost thermal noise diode, which may require additional circuitry and amplifiers to enhance the noise levels; see, for instance, [32] for the implementation of multiple dithering in 12-bit, 18 gigasamples per second (GS/s) ADC.

In particular, time-varying thresholds (random dithering) were considered for the covariance recovery from one-bit measurements in [17]. This was extended in [28] for a significantly improved estimation of signal autocorrelation via the *modified arcsine law*. In non-stationary scenarios, [27] applied the modified arcsine law to utilize time-varying sampling thresholds. Applications of one-bit quantization with time-varying thresholds (dithered one-bit quantization) to diverse problems such as sparse parameter estimation [33], compressed sensing [34], [35], and phase retrieval [26] have also appeared in the contemporary literature.

Evidently, one-bit and unlimited sampling frameworks address complementary requirements. A one-bit ADC only compares an input signal with a given threshold. Therefore, essentially, one-bit sensing is indifferent to DR because, apart from the comparison bit, other information such as the distance between the signal value and the threshold is not stored. On the other hand, the modulo ADC in unlimited sampling provides a natural approach to producing judicious time-varying thresholds for one-bit ADCs. In this paper, to harness advantages of both methods, we propose *unlimited one-bit* (UNO) sampling to design sampling thresholds which are highly informative about the signal of interest.

A. Prior Art

Modulo sampling has also been studied in the context of rate-distortion in [36], wherein quantized modulo samples are reconstructed by linear prediction (LP) and side-information. It was demonstrated in [36], [37] that bandlimited functions can be uniquely characterized by modulo samples, provided that the sampling rate exceeds the Nyquist rate. The reconstruction in [36] assumes that a subset of unfolded samples is known and

prior knowledge of the spectrum is required. This limitation is addressed in the blind reconstruction technique of [38].

Unlimited sampling of finite rate of innovation (FRI) signals was discussed in [39]. Extensions to graph signals [40], multi-channel arrays [41], massive MIMO [42] and sparse outliers (noise) [12] have also been proposed. Reconstruction algorithms have included Itoh's method [10], Fourier Prony's method [12], wavelet-based [11], generalized approximate message passing [43], and local average [44] techniques. Very recently, non-idealities in hardware prototyping were considered in [45], [46]; a computational sampling strategy in the form of *unlimited sampling with hysteresis* [47], [48] was found to be more flexible for circuit design specifications. Unlimited sampling has also been used with event-driven sampling (EDS) [49], [50], wherein the modulo-hysteresis model addresses the DR limitations of an asynchronous sigma-delta modulator (ASDM) that transmits trigger times that capture changes in the input integral from the output of a time encoding machine. Event-driven sampling exclusively records transitions, sampling amplitudes, in contrast to one-bit sensing where both amplitudes and time bins are sampled.

To reconstruct the full-precision signal from the one-bit sampled data, conventional approaches [51], [52] include maximum likelihood estimation (MLE) and weighted least squares. However, these methods have a high computational cost, especially for high-dimensional input signals. To this end, we propose using the randomized Kaczmarz algorithm (RKA) [53], [54], which is an iterative algorithm to solve a system of linear inequalities that arise naturally in the one-bit quantization framework. The RKA is simple to implement and performs comparably with the state-of-the-art optimization methods.

Among prior studies involving both one-bit and unlimited frameworks, state-of-the-art results in [55] proposed *one-bit $\Sigma\Delta$ quantization via unlimited sampling*, whose objective is to shrink the *DR between the input signal and its one-bit samples* (i.e., 1). However, when the ratio of the input signal amplitude to the ADC threshold is large, then the imperfect noise shaping in sigma-delta conversion degrades this reconstruction. Here, to a certain extent, oversampling may help with reducing the reconstruction error. Contrary to this work, our proposed UNO technique focuses on a different problem, i.e., shrinking the *DR between the input signal and the time-varying sampling thresholds*. The one-bit sampling is typically performed at significantly high rates. As a result, the resulting observation inequalities form an overdetermined system. When the difference between the DR of the input signal and that of the thresholds increases, the reconstruction degrades significantly. We show that jointly exploiting both unlimited and one-bit sampling techniques provides a more efficient solution by a considerable reduction of the aforementioned gap.

B. Our Motivations and Contributions

In practice, errors arising from quantization noise degrade the reconstruction quality in unlimited sampling framework. In this context, [6] derived the reconstruction guarantees by including this error as bounded additive noise to the modulo samples.

Contrary to this approach, we consider the more realistic case of additive noise to the input signal.

In this work, we leverage the benefits offered by both unlimited sampling and one-bit quantization. This result is a low-complexity coarse quantization that also effectively addresses the DR limitations typically associated with conventional one-bit ADCs. This entails designing time-varying sampling thresholds for one-bit quantization that closely align with the DR of the modulo samples. In conventional dithered one-bit quantization, the design of thresholds lacks information about the input signal, especially its DR. In contrast, our proposed scheme leverages the modulo operator with a known ADC threshold, allowing us to determine the DR of the modulo samples. This knowledge facilitates the design of thresholds that closely match the DR of the modulo samples, enabling the production of informative one-bit data. This approach holds great potential for applications where the input signal is characterized by very high DRs such as high dynamic range (HDR) imaging [56], [57], [58], sensor array processing [41] and radar remote sensing [59].

Our main contributions in this paper are:

1) Combined unlimited and one-bit sampling framework. In the proposed UNO framework, we leverage upon the benefits of both one-bit and unlimited sampling techniques. The result is a sampling approach that yields unlimited DR and a low-cost, low-power receiver while retaining a high sampling rate. We design time-varying sampling thresholds for one-bit quantization, whose DR is closer to that of the modulo samples. This aids in accurately storing the information of distance between the signal values and thresholds to utilize in the signal reconstruction task. We show that compared to the one-bit reconstruction with random thresholds, our proposed UNO sampling based on time-varying thresholds performs better, especially for high DR signals. Both Gaussian and uniform dithering schemes are widely used in practical quantization systems [30], [60], [61], [62]. To align with existing literature and comprehensively assess the performance of both dithering schemes, we will propose a threshold design method for each of them.

2) RKA-based reconstruction. The signal reconstruction from one-bit measurements requires solving an overdetermined linear feasibility problem that we recast as a one-bit polyhedron and efficiently solve it via the RKA. By generating an abundant number of one-bit samples, we show that the singular values of one-bit data matrix that creates the one-bit polyhedron are equal to the number of dithering sequences employed in one-bit sensing. Further, we numerically investigate the effects of ADC threshold and signal amplitude in the RKA-based UNO reconstruction.

3) Performance guarantees. We showcase the convergence and complexity of our algorithm and leverage the concentration inequality of average distances between signals and dithers to derive an upper bound for the recovery performance in one-bit sensing within the modulo domain.

4) Reconstruction in the presence of additive noise. When the input signal is contaminated with additive noise, we apply

the recently introduced new plug-and-play (PnP) priors [63] to the alternating direction method of multipliers (ADMM) as an additional reconstruction algorithm step. In image denoising problems, the PnP-ADMM is used to replace the shrinkage step of the standard ADMM algorithm with any off-the-shelf algorithm to ensure the noise variance is sufficiently suppressed. Although PnP-ADMM appears *ad hoc*, it yields a better performance than state-of-the-art methods in several different inverse problems [63], [64]. For the noisy UNO, we deploy this algorithm to reconstruct the original signal from overdetermined and underdetermined noisy systems. Moreover, we show that the additive noise to the input signal contaminates the modulo samples with noise that is expressed in terms of the input noise.

C. Organization and Notations

In the next section, we provide an introduction to one-bit quantization with time-varying sampling thresholds. Particularly, the one-bit sampled signal reconstruction problem is formulated as an overdetermined system of linear inequalities. We describe one-bit signal reconstruction and introduce RKA in Section III. Then, Section IV recalls the concept of unlimited sampling [6], [10] and proposes UNO to design judicious thresholds and guarantee the one-bit signal reconstruction in the high-DR. In Section V, we provide several numerical experiments to illustrate UNO-based sampling and analyze the reconstruction error. We consider the noisy measurement scenario in Section VI and conclude in Section VII.

Throughout this paper, we use boldface lowercase, boldface uppercase, and calligraphic letters for vectors, matrices, and sets, respectively. The notations \mathbb{C} , \mathbb{R} , and \mathbb{Z} represent the set of complex, real, and integer numbers, respectively. We represent a vector \mathbf{x} in terms of its elements $\{x_i\}$ or $(\mathbf{x})_i$ as $\mathbf{x} = [x_i]$. We use $(\cdot)^\top$ and $(\cdot)^H$ to denote the vector/matrix transpose and the Hermitian transpose, respectively. We define $\mathbf{x} \succeq \mathbf{y}$ as a component-wise inequality between vectors \mathbf{x} and \mathbf{y} , i.e., $x_i \geq y_i$ for every index i [65, p. 32]. The identity matrix of size N is $\mathbf{I}_N \in \mathbb{R}^{N \times N}$. The Frobenius norm of a matrix $\mathbf{B} \in \mathbb{C}^{M \times N}$ is defined as $\|\mathbf{B}\|_F = \sqrt{\sum_{r=1}^M \sum_{s=1}^N |b_{rs}|^2}$, where b_{rs} is the (r, s) -th entry of \mathbf{B} . The function $\text{diag}(\cdot)$ outputs a diagonal matrix with the input vector along its main diagonal. The ℓ_p -norm of a vector \mathbf{b} is $\|\mathbf{b}\|_p = (\sum_i b_i^p)^{1/p}$. The infinity or max-norm of a function x is $\|x\|_\infty = \inf \{c_0 \geq 0 : |x(t)| \leq c_0\}$, where $\inf(\cdot)$ denotes the infimum of its argument; for vectors, we have $\|\mathbf{x}\|_\infty = \max_k |x_k|$. For a vector \mathbf{x} , $\Delta \mathbf{x} = x_{k+1} - x_k$ denotes the finite difference and recursively applying the same yields N -th order difference, $\Delta^N \mathbf{x}$. We denote the Ω -bandlimited Paley-Wiener subspace of the square-integrable function space L^2 by PW_Ω such that $\text{PW}_\Omega = \{f : f, \hat{f} \in L^2, \text{supp}(f) \subset [-\Omega, \Omega]\}$, where \hat{f} is the Fourier transform of f . The Hadamard (element-wise) product of two matrices \mathbf{B}_1 and \mathbf{B}_2 is $\mathbf{B}_1 \odot \mathbf{B}_2$. The column-wise vectorized form of a matrix \mathbf{B} is $\text{vec}(\mathbf{B})$. Given a scalar x , we define the operator $(x)^+$ as $\max\{x, 0\}$. For an event \mathcal{E} , $\mathbb{1}_{(\mathcal{E})}$ is the indicator function for that event meaning that $\mathbb{1}_{(\mathcal{E})}$ is 1 if \mathcal{E} occurs; otherwise, it is zero. The function $\text{sgn}(\cdot)$ yields the sign of its argument. In the context of

numerical computations, $\lfloor \cdot \rfloor$ and $\lceil \cdot \rceil$ denote the floor and ceiling functions, respectively. The function $\log(\cdot)$ denotes the natural logarithm, unless its base is otherwise stated. The notation $x \sim \mathcal{U}(a, b)$ means a random variable drawn from the uniform distribution over the interval $[a, b]$ and $x \sim \mathcal{N}(\mu, \sigma^2)$ represents the normal distribution with mean μ and variance σ^2 . The operator $\text{mod}(a, b)$ between two values a and b , returns the remainder of the division operation a/b . A ball with radius r centered at a point $\mathbf{y} \in \mathbb{R}^n$ is defined as $\mathcal{B}_r(\mathbf{y}) = \{\mathbf{y}_1 \in \mathbb{R}^n \mid \|\mathbf{y} - \mathbf{y}_1\|_2 \leq r\}$.

II. ONE-BIT QUANTIZATION: OVERDETERMINED LINEAR SYSTEM FORMULATION

Several approaches have been proposed in the literature to reconstruct the signal of interest from one-bit samples with the most of them formulating this task as an optimization problem. For example, the covariance matrix formulation of [30] employs the cyclic optimization method to recover the parameters. A convex program based on the Gauss-Legendre integration to recover the input covariance matrix from one-bit sampled data was suggested in [13], [27], [28]. Other recent works exploit sparsity of the signal and apply techniques such as ℓ_1 -norm minimization [66], [67], ℓ_1 -regularized MLE formulation [51], [52], and log-relaxation [68] to lay the ground for signal reconstruction. In the following, we explain our one-bit polyhedron formulation, wherein a strong efficient and easily implementable solver of linear feasibility problems is applied to the aforementioned application-specific methods.

A. One-Bit Quantization Using Time-Varying Thresholds

Consider a bandlimited continuous-time signal $x \in \text{PW}_\Omega$ that we represent via Shannon's sampling theorem as [69]

$$0 < T \leq \frac{\pi}{\Omega}, \quad x(t) = \sum_{k=-\infty}^{k=+\infty} x(kT) \text{sinc}\left(\frac{t}{T} - k\right), \quad (1)$$

where $1/T$ is the sampling rate, Ω is the signal bandwidth, and $\text{sinc}(t) = \frac{\sin(\pi t)}{\pi t}$ is an *ideal* low-pass filter. Denote the uniform samples of $x(t)$ with the sampling rate $1/T$ by $x_k = x(kT)$.

In practice, the discrete-time samples occupy pre-determined quantized values. We denote the quantization operation on $x[k]$ by the function $Q(\cdot)$. This yields the quantized signal as $r_k = Q(x_k)$. In one-bit quantization, compared to zero or constant thresholds, time-varying sampling thresholds yield a better reconstruction performance [13], [27]. These thresholds may be chosen from any distribution. In this work, we consider a Gaussian non-zero time-varying threshold vector $\boldsymbol{\tau}_\mathcal{N} = [\tau_k]$ that follows the distribution $\boldsymbol{\tau}_\mathcal{N} \sim \mathcal{N}(\mathbf{d} = \mathbf{1}d, \boldsymbol{\Sigma})$. Following a bell-shaped distribution, a Gaussian threshold is likely to be concentrated in the center and may not cover the entire signal range accurately. Therefore, alternatively, we also employ uniformly distributed thresholds in the sequel as $\boldsymbol{\tau}_\mathcal{U} \sim \mathcal{U}_{[a,b]}$ with upper b and lower a bounds. For one-bit quantization with such time-varying sampling thresholds, $r_k = \text{sgn}(x_k - \tau_k)$. For notational simplicity, hereafter, we denote the time-varying sampling thresholds by dropping the subscripts, i.e. $\boldsymbol{\tau} = [\tau_k]$.

B. One-Bit Polyhedron

The information gathered through the one-bit sampling with time-varying thresholds may be formulated in terms of an overdetermined linear system of inequalities. We have $r_k = +1$ when $x_k > \tau_k$ and $r_k = -1$ when $x_k < \tau_k$. Collecting all the elements in the vectors as $\mathbf{x} = [x_k] \in \mathbb{R}^n$ and $\mathbf{r} = [r_k] \in \mathbb{R}^n$, therefore, one can formulate the geometric location of the signal as $r_k(x_k - \tau_k) \geq 0$, whose vectorized representation is $\mathbf{r} \odot (\mathbf{x} - \boldsymbol{\tau}) \geq \mathbf{0}$ or equivalently

$$\boldsymbol{\Omega} \mathbf{x} \succeq \mathbf{r} \odot \boldsymbol{\tau}, \quad (2)$$

where $\boldsymbol{\Omega} \triangleq \text{diag}(\mathbf{r})$. Suppose $\mathbf{x}, \boldsymbol{\tau} \in \mathbb{R}^n$, and that $\boldsymbol{\tau}^{(\ell)}$ denotes the time-varying sampling threshold in ℓ -th signal sequence, where $\ell \in [m]$.

For the ℓ -th signal sequence, (2) becomes

$$\boldsymbol{\Omega}^{(\ell)} \mathbf{x} \succeq \mathbf{r}^{(\ell)} \odot \boldsymbol{\tau}^{(\ell)}, \quad \ell \in [m], \quad (3)$$

where $\boldsymbol{\Omega}^{(\ell)} = \text{diag}(\mathbf{r}^{(\ell)})$. Denote the concatenation of all m sign matrices as

$$\tilde{\boldsymbol{\Omega}} = [\boldsymbol{\Omega}^{(1)} \mid \dots \mid \boldsymbol{\Omega}^{(m)}]^\top, \quad \in \mathbb{R}^{mn \times n}. \quad (4)$$

Rewrite the m linear system of inequalities in (3) as

$$\tilde{\boldsymbol{\Omega}} \mathbf{x} \succeq \text{vec}(\mathbf{R}) \odot \text{vec}(\boldsymbol{\Gamma}), \quad (5)$$

where \mathbf{R} and $\boldsymbol{\Gamma}$ are matrices, whose columns are the sequences $\{\mathbf{r}^{(\ell)}\}_{\ell=1}^m$ and $\{\boldsymbol{\tau}^{(\ell)}\}_{\ell=1}^m$, respectively.

The linear system of inequalities in (5) associated with the one-bit sampling scheme is overdetermined. We recast (5) into a *one-bit polyhedron* as

$$\mathcal{P} = \left\{ \mathbf{x} \mid \tilde{\boldsymbol{\Omega}} \mathbf{x} \succeq \text{vec}(\mathbf{R}) \odot \text{vec}(\boldsymbol{\Gamma}) \right\}. \quad (6)$$

Leveraging upon the benefits of one-bit quantization, with an increase in the number of samples, the space constrained by the one-bit polyhedron $\mathcal{P}_\mathbf{x}$ progressively shrinks and remains contained within the feasible set. This shrunken space always encompasses the global minima, with a volume that decreases with an increase in the sample size. Instead of complex high-dimensional optimization with techniques such as MLE, our objective is to employ the polyhedron (6) that encapsulates the desired signal \mathbf{x} and leads to solving linear inequalities with linear convergence in expectation.

III. ONE-BIT SIGNAL RECONSTRUCTION

To reconstruct \mathbf{x} from the sign data $\{\mathbf{r}^{(\ell)}\}_{\ell=1}^m$, we solve the polyhedron search problem through RKA because of its optimal projection and linear convergence in expectation [26], [54].

A. RKA

The RKA is a *subconjugate gradient method* to solve overdetermined linear systems, i.e. $\mathbf{C}\mathbf{x} \leq \mathbf{b}$ where \mathbf{C} is a $m' \times n'$ matrix with $m' > n'$ [53], [54]. The conjugate-gradient methods turn this inequality to an equality of the following form

$(\mathbf{C}\mathbf{x} - \mathbf{b})^+ = 0$, and then solve it as any other system of equations. Given a sample index set $[m']$, without loss of generality, rewrite linear feasibility as the polyhedron

$$\begin{cases} \mathbf{c}_j \mathbf{x} \leq b_j & (j \in \mathcal{I}_{\leq}), \\ \mathbf{c}_j \mathbf{x} = b_j & (j \in \mathcal{I}_{=}), \end{cases} \quad (7)$$

where $\{\mathbf{c}_j\}$ are the rows of \mathbf{C} and the disjoint index sets \mathcal{I}_{\leq} and $\mathcal{I}_{=}$ partition $[m']$. The projection coefficient β_i of the RKA is [53], [54]:

$$\beta_i = \begin{cases} (\mathbf{c}_j \mathbf{x}_i - b_j)^+ & (j \in \mathcal{I}_{\leq}), \\ \mathbf{c}_j \mathbf{x}_i - b_j & (j \in \mathcal{I}_{=}). \end{cases} \quad (8)$$

The unknown column vector \mathbf{x} is iteratively updated as

$$\mathbf{x}_{i+1} = \mathbf{x}_i - \frac{\beta_i}{\|\mathbf{c}_j\|_2} \mathbf{c}_j^H, \quad (9)$$

where, at each iteration i , the index j is drawn from the set $[m']$ independently at random following the distribution $\Pr\{j = k\} = \frac{\|\mathbf{c}_k\|_2^2}{\|\mathbf{C}\|_F^2}$. Note that, (6) has only the inequality partition \mathcal{I}_{\leq} . Herein, $m' = m \times n$ and $n' = n$. The row vector \mathbf{c}_j and the scalar b_j in the RKA (7)-(9) are j -th row of $-\tilde{\Omega}$ and j -th element of $-(\text{vec}(\mathbf{R}) \odot \text{vec}(\mathbf{\Gamma}))$, respectively. It may be readily verified that the distribution of choosing a specific sample index j for the inequalities in (6) is uniform, i.e., $\Pr\{j = k\} = \frac{1}{mn}$.

In one-bit reconstruction, $\mathbf{c}_j = -\omega_j$, wherein ω_j is the j -th row of $\tilde{\Omega}$; a j' -th coordinate vector with ± 1 as its j' -th element and

$$j' = \begin{cases} \text{mod}(j, n), & j \neq kn, \\ n, & j = kn, \end{cases} \quad (10)$$

with $1 \leq k \leq m$. This property makes the update process (9) similar to that of the *randomized Gauss-Seidal* method using the coordinate vector in each iteration [54], [70]. This approach is commonly used for solving high-dimensional linear feasibility problems by updating only one dimension at any iteration. The structure of matrix $\tilde{\Omega}$ leads to a similar efficient RKA implementation by updating only the generic element j' at each iteration, i.e., $(\mathbf{x}_{i+1})_{j'} = (\mathbf{x}_i)_{j'} - \beta_i r_{j'}$, where $r_{j'}$ is the one-bit data at index j' .

B. Convergence Analysis of RKA

At the i -th iteration, the error between the RKA estimate \mathbf{x}_i and a solution inside the feasible set $\hat{\mathbf{x}}$ has been shown to follow the convergence bound [53], [54], [71]

$$\mathbb{E} \left\{ \|\mathbf{x}_i - \hat{\mathbf{x}}\|_2^2 \right\} \leq q^i \|\mathbf{x}_0 - \hat{\mathbf{x}}\|_2^2, \quad (11)$$

where $q = 1 - \frac{1}{\kappa(\tilde{\Omega})} \in (0, 1)$ and $\kappa(\tilde{\Omega}) = \|\tilde{\Omega}\|_F^2 \|\tilde{\Omega}^\dagger\|_2^2$ is *scaled condition number* [72] of $\tilde{\Omega}$, which is a block matrix of m diagonal matrices per (4). We have

$$\|\tilde{\Omega}\|_F^2 = \sum_{j=1}^{mn} r_j^2 = \sum_{j=1}^{mn} 1 = mn. \quad (12)$$

Moreover, $\|\tilde{\Omega}^\dagger\|_2^2 = \frac{1}{\sigma_{\min}^2}$, where $\sigma_{\min} = \min\{\sigma_i\}$ is the minimum singular value of $\tilde{\Omega}$ [73] (maximum singular value is σ_{\max} similarly defined). Following Lemma 1 evaluates singular values of $\tilde{\Omega}$.

Lemma 1: Consider the concatenation of all m sign data matrices in (4), i.e., $\tilde{\Omega} \in \mathbb{R}^{mn \times n}$, where n is the size of the input signal and m is the number of time-varying sampling thresholds. The matrix $\tilde{\Omega}$ is full-rank and its singular values are $\sigma_1 = \sigma_2 = \dots = \sigma_n = \sqrt{m}$.

Proof: Compute the square matrix

$$\begin{aligned} \mathbf{P} &= \tilde{\Omega}^\top \tilde{\Omega} = [\Omega^{(1)} | \dots | \Omega^{(m)}] [\Omega^{(1)} | \dots | \Omega^{(m)}]^\top \\ &= \Omega^{(1)} (\Omega^{(1)})^\top + \Omega^{(2)} (\Omega^{(2)})^\top + \dots + \Omega^{(m)} (\Omega^{(m)})^\top, \\ &= m\mathbf{I}. \end{aligned} \quad (13)$$

Hence, the eigenvalues of \mathbf{P} are equal to m . In other words, the singular values of $\tilde{\Omega}$ are $\{\sigma_i\}_{i=1}^n = \sqrt{m}$. ■

It follows from (12) and Lemma 1 that $\kappa(\tilde{\Omega}) = \frac{mn}{\sigma_{\min}^2} = n$. leads to $q = \frac{n-1}{n}$. Set the algorithm termination criterion to the condition

$$\mathbb{E} \left\{ \|\mathbf{x}_i - \hat{\mathbf{x}}\|_2^2 \right\} \leq \epsilon_1 \|\mathbf{x}_0 - \hat{\mathbf{x}}\|_2^2, \quad (14)$$

where ϵ_1 is a positive constant. Based on this criterion and (11), the following Proposition 1 states the order of the number of required RKA iterations.

Proposition 1: The number of RKA iterations i required to achieve a solution inside the one-bit polyhedron $\hat{\mathbf{x}}$ of length n from its one-bit samples within the error specified by (14) is $i = \mathcal{O} \left(n \log \left(\frac{1}{\epsilon_1} \right) \right)$, where ϵ_1 is a positive constant.

Proof: Define $q^i \|\mathbf{x}_0 - \hat{\mathbf{x}}\|_2^2 \leq \epsilon_1 \omega_0$, or equivalently,

$$q^i \leq \epsilon_1. \quad (15)$$

Note that ω_0 is a constant scalar that depends on only the initial and optimal solutions and since the error decreases during the iterations in the RKA, we have $\epsilon_1 \leq \omega_0$. Using (15) and taking logarithm on both sides yields

$$i \geq \frac{\log(\epsilon_1)}{\log(1 - \frac{1}{n})}. \quad (16)$$

The right-hand side of (16) can be approximated by [53]:

$$\frac{\log(\epsilon_1)}{\log(1 - \frac{1}{n})} \approx n \log \left(\frac{1}{\epsilon_1} \right), \quad (17)$$

which completes the proof. ■

C. Numerical Example

Figure 1(a) illustrates the RKA reconstruction of a sawtooth signal from one-bit polyhedron in (6) for 10 sweeps (periods) with a fundamental frequency of 50 Hz. We discretized the generated signal $x(t)$ at the sampling rate (interval) of 1 kHz ($T = 0.001$ s). The time-varying sampling thresholds were drawn from the distribution $\tau^{(\ell)} \sim \mathcal{N}(\mathbf{0}, \mathbf{I})$, for all $\ell \in [m]$. Define the normalized squared error, $\text{NSE} \triangleq \frac{\|\mathbf{x} - \hat{\mathbf{x}}\|_2^2}{\|\mathbf{x}\|_2^2}$, where \mathbf{x} and $\hat{\mathbf{x}}$ denote the true (discretized) signal and its reconstructed version,

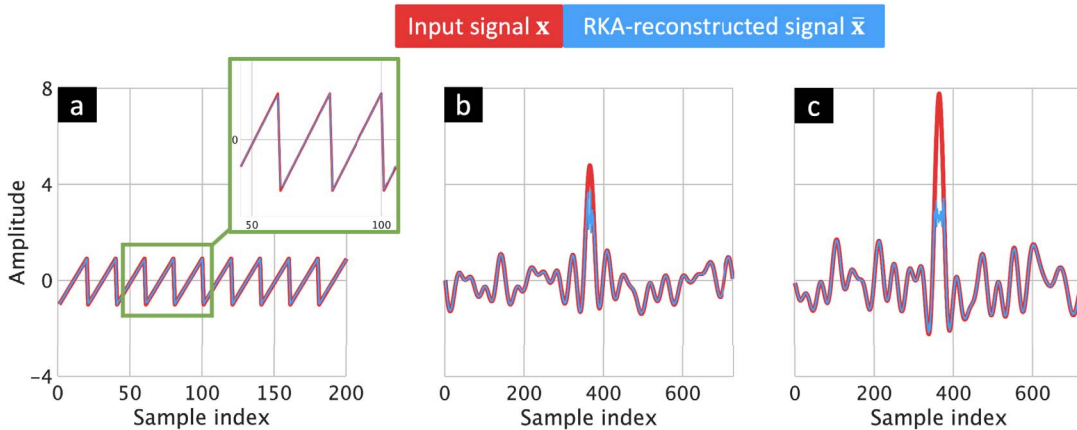


Figure 1. (a) The input sawtooth wave signal \mathbf{x} is reconstructed from one-bit measurements using the RKA to yield $\bar{\mathbf{x}}$. Here, $\text{DR}_{\mathbf{x}} = 1$ and $\text{DR}_{\tau} = 1$. The inset shows the same plot on a larger scale. (b) As in (a) but for the bandlimited input signal from [6] with $\text{DR}_{\mathbf{x}} = 5$. (c) As in (b) but for $\text{DR}_{\mathbf{x}} = 8$.

respectively. Since RKA selects each hyperplane randomly in each iteration, we repeat the reconstruction in Figure 1(a) for 1000 times. The averaged NSE (normalized mean squared error denoted by NMSE) over all experiments is only ~ 0.0012 or -29.2082 dB.

D. Limitations of Conventional One-Bit Reconstruction

Denote the DRs of the desired signal \mathbf{x} and the time-varying threshold τ by $\text{DR}_{\mathbf{x}}$ and DR_{τ} , respectively, where we define the DR of a vector as its ℓ_{∞} -norm. If $\text{DR}_{\mathbf{x}} \leq \text{DR}_{\tau}$, then the reconstructed signal \mathbf{x}^* may be found inside the polyhedron (6) with a high probability for an adequate number of samples. Otherwise, if $\text{DR}_{\mathbf{x}} > \text{DR}_{\tau}$, there is no guarantee to obtain \mathbf{x}^* since the desired solution cannot be inside the finite-volume space imposed by the set of inequalities in (6) indicating an irretrievable information loss. We demonstrate this as follows. Without loss of generality, consider $x_k = \text{DR}_{\mathbf{x}}$ for $x_k > 0$. Assume $\tau_k^* = \max_{\ell} \tau_k^{(\ell)}$. Since $\text{DR}_{\tau} = \|\tau\|_{\infty}$, we have $\tau_k^* \leq \text{DR}_{\tau}$. If $\text{DR}_{\mathbf{x}} > \text{DR}_{\tau}$, then we have $\tau_k^* < \text{DR}_{\mathbf{x}} = x_k$. Therefore, to reconstruct the k -th entry of the input signal x_k , we always have a gap $\delta = x_k - \tau_k^* > 0$ that is not covered by any sample to capture the amplitude information of \mathbf{x} . Hence, the desired signal is not found inside the finite-volume space imposed by the inequalities in (6).

In Figure 1(a), $\text{DR}_{\tau} = 3$ is larger than $\text{DR}_{\mathbf{x}} = 1$ thereby leading to a low reconstruction NMSE. We now consider x to be a bandlimited function with piece-wise constant Fourier transform values are drawn uniformly at random, i.e., $\hat{x}(\omega) \sim \text{unif}(0, 1)$. This signal is the same as the one used in [6]. The time-varying sampling thresholds were generated following the procedure explained in this section. Figure 1(b) shows the RKA-based reconstruction of the bandlimited signal from the polyhedron (6). Around $t = 0$ (corresponding sample index is 364 in the plot), the reconstruction severely degrades because $\text{DR}_{\mathbf{x}} = 5$ is set to be larger than $\text{DR}_{\tau} = 3$. Indeed, when the difference between $\text{DR}_{\mathbf{x}}$ and DR_{τ} increases further, we observe a significant loss of information in the reconstructed signal (Figure 1(c)).

IV. UNO SAMPLING

Modulo sampling suggests that instead of point-wise samples of the bandlimited function $x(t)$, the signal is digitized using a modulo ADC with a predefined threshold $\lambda > 0$ such that any signal value outside the range $[-\lambda, \lambda]$ is *folded* to the same range [6], [10]. For practical implementations and theoretical analysis of the modulo ADCs, we refer the interested reader to [12], [45]. The folding corresponds to introducing a non-linearity in the sensing process [6], [10]. We denote the folding by the modulo operator \mathcal{M}_{λ} that represents the following mapping:

$$\mathcal{M}_{\lambda}(x_k) : \tilde{x}_k = x_k - 2\lambda \left\lfloor \frac{x_k}{2\lambda} + \frac{1}{2} \right\rfloor, \quad (18)$$

where \tilde{x}_k are the modulo samples of $x(t)$.

A. Unlimited Sensing

The *unlimited sampling theorem* [6] (reproduced below) states that, if the estimate of the norm of the bandlimited signal is known, then its perfect reconstruction (up to additive multiples of 2λ) from its modulo samples is possible with at least sampling period $T \leq (2\pi e)^{-1}$, where e is the Euler's number and the signal bandwidth has been normalized to π .

Theorem 1 (Unlimited sampling theorem [6]): Assume $x(t)$ to be a finite energy, bandlimited signal with maximum frequency Ω_{\max} and let $\tilde{x}_k, k \in \mathbb{Z}$ in (18) be the modulo samples of $x(t)$ with sampling rate $1/T$. Then a sufficient condition for the reconstruction of $x(t)$ from $\{\tilde{x}_k\}$ is that $T \leq \frac{1}{2\Omega_{\max} e}$ (up to additive multiples of 2λ).

Theorem 1 implies that the sampling rate depends on only the bandwidth and is independent of the ratio of ADC threshold λ to the signal amplitude. In other words, the DR of the input signal is *unlimited*. Recently, stable unlimited sampling reconstruction in the presence of noise has also been obtained [6].

The reconstruction of the bandlimited function $x(t)$ from its modulo samples $\{\tilde{x}_k\}$ is achieved as follows. Assume that $x(t)$ admits a decomposition [6], [10],

$$x(t) = \tilde{x}(t) + \epsilon_x(t), \quad (19)$$

Algorithm 1 Input signal reconstruction from modulo folded samples.

Input: $\tilde{x}_k = \mathcal{M}_\lambda(x_k)$, ADC threshold λ , and $2\lambda\mathbb{Z} \ni \beta_x \geq \|x\|_\infty$.
Output: The reconstruction of the input signal \bar{x} .

- 1: $N \leftarrow \left\lceil \frac{\log \lambda - \log \beta_x}{\log(T\Omega e)} \right\rceil$ using (22).
- 2: $\Delta^N \epsilon_x \leftarrow \mathcal{M}_\lambda(\Delta^N \tilde{\mathbf{x}}) - \Delta^N \tilde{\mathbf{x}}$.
- 3: $\mathbf{s}_0 \leftarrow \Delta^N \epsilon_x$.
- 4: **for** $p = 0 : N - 2$ **do**
- 5: $\mathbf{s}_{p+1} \leftarrow \nabla \mathbf{s}_p \triangleright \nabla$ is the inverse-difference operator defined in (21).
- 6: $\mathbf{s}_{p+1} \leftarrow 2\lambda \left\lceil \frac{\lfloor \mathbf{s}_{p+1} / \lambda \rfloor}{2} \right\rceil \triangleright$ rounding to $2\lambda\mathbb{Z}$.
- 7: $\kappa_p \leftarrow \left\lceil \frac{(\nabla^2 \Delta^p \epsilon_x)_1 - (\nabla^2 \Delta^p \epsilon_x)_{J+1}}{12\beta_x} + \frac{1}{2} \right\rceil \triangleright J = \frac{6\beta_x}{\lambda}$.
- 8: $\mathbf{s}_{p+1} \leftarrow \mathbf{s}_{p+1} + 2\lambda\kappa_p$.
- 9: **return** $\bar{\mathbf{x}} \leftarrow \nabla \mathbf{s}_{N-1} + \tilde{\mathbf{x}} + 2a\lambda, \quad a \in \mathbb{Z}$.

where $\tilde{x}(t) = \mathcal{M}_\lambda(x(t))$ and the error ϵ_x between the input signal and its modulo samples is

$$\epsilon_x(t) = 2\lambda \sum_{u \in \mathbb{Z}} e_u \mathbb{1}_{\mathcal{D}_u}(t), \quad e_u \in \mathbb{Z}, \quad (20)$$

where $\bigcup_{u \in \mathbb{Z}} \mathcal{D}_u = \mathbb{R}$ is a partition of the real line into intervals \mathcal{D}_u . As indicated by (19), if ϵ_x is known, then x can be reconstructed from \tilde{x} . It follows from (20) that ϵ_x takes only those values that are integer multiples of 2λ thereby leading to a robust reconstruction algorithm [6]. To obtain ϵ_x (up to an unknown additive constant) and subsequently the desired signal $x(t)$, the reconstruction procedure in [6], [10] requires the higher-order differences of $\tilde{\mathbf{x}} = [\tilde{x}_k]$ to obtain $\Delta^N \epsilon_x = \mathcal{M}_\lambda(\Delta^N \tilde{\mathbf{x}}) - \Delta^N \tilde{\mathbf{x}}$, where $\epsilon_x = [\epsilon_x]$. Define the inverse-difference operator as a sum of real sequence $\{s_b\}$, i.e.,

$$\nabla : \{s_k\}_{k \in \mathbb{Z}^+} \rightarrow \sum_{b=1}^k s_b. \quad (21)$$

Then, applying $\nabla(\Delta^N \epsilon_x)$ and rounding the result to the nearest multiple of $2\lambda\mathbb{Z}$ yields ϵ_x . For a guaranteed and stable reconstruction performance, a suitable choice for difference order N is [6],

$$N \geq \left\lceil \frac{\log \lambda - \log \beta_x}{\log(T\Omega e)} \right\rceil, \quad (22)$$

where β_x is chosen such that $\beta_x \in 2\lambda\mathbb{Z}$ and $\|x\|_\infty \leq \beta_x$. Algorithm 1 summarizes the unlimited sampling reconstruction procedure.

B. Towards a Reconstruction Guarantee for One-Bit Sensing

Since linear feasibility problem solvers do not guarantee a good signal reconstruction from one-bit measurements in (6) when the DR of the signal exceeds that of the time-varying

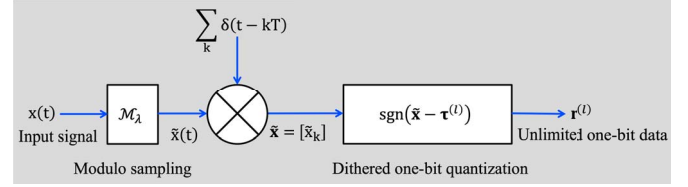


Figure 2. The UNO sampling architecture. The proper choice of the sampling interval T in the middle block is specified by Theorem 3.

sampling threshold, it is pertinent to design the time-varying sampling threshold such that $\text{DR}_x \leq \text{DR}_\tau$. This is not always possible because the desired signal is unknown. We address this limitation via UNO, which is our proposed new one-bit sensing method based on the concept of modulo sampling. Modulo sampling offers a natural approach to designing dithers in a manner that fully covers the dynamic range of input measurements in the memoryless scalar quantization system.

As discussed in Section IV-A, unlimited sampling yields signal amplitudes folded within the range $[-\lambda, \lambda]$. This suggests an alternative time-varying threshold with the same DR as the modulo samples $\tilde{\mathbf{x}} = [\tilde{x}_k]$; i.e. $\text{DR}_\tau = \lambda$. In other words, the thresholds are modified to be closer to the clipping value and the modulo ADC is integrated with one-bit sampling. We summarize this UNO sampling framework as follows:

- 1) Apply the modulo operator defined in (18) to the input signal \mathbf{x} and obtain modulo samples $\tilde{\mathbf{x}} = \mathcal{M}_\lambda(\mathbf{x})$.
- 2) Design sequences of the time-varying sampling threshold $\{\tau^{(\ell)}\}_{\ell=1}^m$ such that $|\text{DR}_{\tau^{(\ell)}} - \lambda| \leq \varepsilon_0$ for all $\ell \in [m]$ and a small number ε_0 .
- 3) Apply the one-bit quantization to modulo samples as $\mathbf{r}^{(\ell)} = \text{sgn}(\tilde{\mathbf{x}} - \tau^{(\ell)})$.

Figure 2 illustrates various steps of our UNO sampling technique. In order to derive a guarantee for the UNO threshold, we introduce a useful lemma as follows.

Lemma 2: Assume $\tau^{(\ell)} \sim \mathcal{N}(\mathbf{0}, \sigma_\tau^2 \mathbf{I})$. Then, with probability at least $1 - \eta$, we have

$$\|\tau^{(\ell)}\|_\infty \leq \sigma_\tau \sqrt{2 \log \left(\frac{2n}{\eta} \right)}. \quad (23)$$

Proof: According to the Hoeffding inequality and union bound for the Gaussian random variables $\tau^{(\ell)} \sim \mathcal{N}(\mathbf{0}, \sigma_\tau^2 \mathbf{I})$, we have [74]

$$\Pr \left(\|\tau^{(\ell)}\|_\infty \geq t \right) \leq 2n e^{-\frac{t^2}{2\sigma_\tau^2}}. \quad (24)$$

Therefore, with $2n e^{-\frac{t^2}{2\sigma_\tau^2}} \leq \eta$ proving the lemma. \blacksquare

The following Proposition 2 states the UNO threshold design.

Proposition 2 (Judicious threshold design: Gaussian dithering): Under the UNO sampling framework, the following DR guarantee holds: Assume each one-bit sampling threshold $\tau^{(\ell)} \in \mathbb{R}^n$ is distributed as $\tau^{(\ell)} \sim \mathcal{N}(\mathbf{0}, \sigma_\tau^2 \mathbf{I})$. Then, considering the ADC threshold λ , σ_τ will be equal to $\frac{\lambda}{\sqrt{2 \log \left(\frac{2n}{\eta} \right)}}$ with a probability of at least $1 - \eta$.

Proof: With a probability of at least $1 - \eta$, the maximum amplitude of each threshold sequence is obtained via Lemma 2.

When $\sigma_\tau = \frac{\lambda}{\sqrt{2 \log(\frac{2n}{\eta})}}$, then time-varying sampling threshold also has a DR of λ with a probability of at least $1 - \eta$. ■

In Proposition 2, we design time-varying sampling threshold sequences so that their DR is close to that of the modulo samples. This enables storing the information on the distance between the modulo signal and the thresholds without any loss of information via one-bit sampling. The DR of the threshold should fall within the range of the ADC threshold with high probability. Further, the threshold should cover the entire DR of modulo samples between $-\lambda$ and λ . The condition stated in Proposition 2 guarantees that the DR of the threshold aligns with the ADC threshold range. However, in practical scenarios, it is conceivable that this condition may not encompass the entire DR of modulo samples because the Gaussian distribution (with a bell-shaped curve) concentrates the majority of data towards its boundaries, which can be narrower than the bound derived from the proposition.

In practice, it might be necessary to choose a threshold variance that exceeds the value indicated by Proposition 1 to ensure adequate coverage of the entire DR of modulo samples. We, therefore, introduce a threshold design method specifically tailored for uniformly distributed thresholds in the following Proposition 3.

Proposition 3 (Judicious threshold design: Uniform dithering): Under the UNO sampling framework, the following dynamic range guarantees hold when $\tau^{(\ell)} \sim \mathcal{U}_{[-a,a]}$, then $\lambda = a$ with a probability of 1.

Proof: The proof for the uniform threshold follows Proposition 2 except that, for each ℓ , we have $\text{DR}_{\tau^{(\ell)}} \leq a$ with a probability of 1 leading to $a = \lambda$. ■

Proposition 3 encompasses both the necessary and sufficient conditions for designing thresholds in the uniform dithering scenario. It ensures that the DR of the threshold aligns with the ADC threshold range, while also covering the DR of the modulo samples.

Figure 3 shows a comparison of conventional one-bit sensing and UNO for the high DR scenario; the transfer function of the former is plotted in Figure 3(a). We consider the same bandlimited signal as in Section III-D and a random threshold $\tau \sim \mathcal{N}(0, \mathbf{I})$. In case of one-bit sensing, the signal values and dithers differ considerably at some points (Figure 3(b)) and, consequently, the information on the distance between the signal value and the threshold samples is completely lost. For UNO, the threshold is chosen closer to the folded signal with $\lambda = 0.5$ (Figure 3(c)). This preserves the information of the input signal in the modulo samples (Figure 3(d)).

For reconstruction of the signal of interest \mathbf{x} from UNO samples, we reformulate the polyhedron (6) for modulo samples as

$$\tilde{\mathcal{P}} = \left\{ \tilde{\mathbf{x}} \mid \tilde{\mathbf{\Omega}}\tilde{\mathbf{x}} \succeq \text{vec}(\mathbf{R}) \odot \text{vec}(\mathbf{\Gamma}) \right\}. \quad (25)$$

This overdetermined system of linear inequalities in (25) is then solved via RKA and, from the resulting reconstructed modulo samples, we obtain \mathbf{x} via Algorithm 1. Algorithm 2 summarizes these steps of the *UNO algorithm*.

Figure 4 shows that increasing the number m of time-varying sampling threshold sequences guarantees the RKA-based

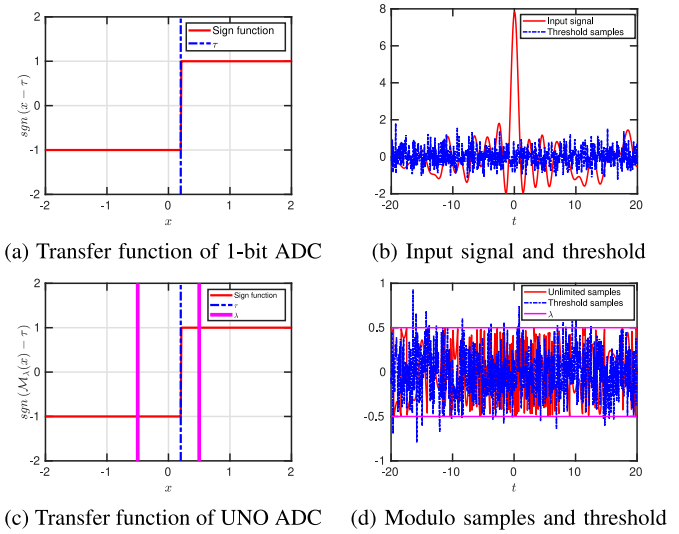


Figure 3. (a) Transfer function of conventional one-bit ADC where the i -th element of the input signal $\mathbf{x} = (\mathbf{x})_i$ is compared with a randomly selected threshold τ . (b) High DR input signal \mathbf{x} and its thresholds samples τ . (c) As in (a), but for UNO with the judicious time-varying threshold $\tau \sim \mathcal{U}_{[-\lambda,\lambda]}$. (d) The modulo samples $\tilde{\mathbf{x}}$ compared with the designed random dithers.

Algorithm 2 Signal reconstruction in UNO.

Input: Sequences of one-bit measurements $\{\mathbf{r}^{(\ell)} = \text{sgn}(\mathcal{M}_\lambda(\mathbf{x}) - \tau^{(\ell)})\}_{\ell=1}^m$, $\tau_{\mathcal{N}}^{(\ell)} \sim \mathcal{N}(\mathbf{0}, \sigma_\tau^2 \mathbf{I})$ (for Gaussian dithering), $\tau_{\mathcal{U}}^{(\ell)} \sim \mathcal{U}_{[-a,a]}$ (for Uniform dithering), minimum probability η , ADC threshold λ , total number of iterations i_{\max} .

Output: The reconstruction of the input signal $\tilde{\mathbf{x}} \in \mathbb{R}^n$.

- 1: $\sigma_\tau \leftarrow \frac{\lambda}{\sqrt{2 \ln\left(\frac{2n}{\eta}\right)}} \triangleright$ For Gaussian dithering.
- 2: $a \leftarrow \lambda \triangleright$ For Uniform dithering.
- 3: Find the modulo signal in $\tilde{\mathcal{P}}$ via RKA.
- 4: **for** $i = 1 : i_{\max}$ **do**
- 5: $\tilde{\mathbf{x}}_{i+1} \leftarrow \tilde{\mathbf{x}}_i + (-\omega_j \tilde{\mathbf{x}}_i + \omega_j \tau^{(\ell)})^+ \omega_j^\top$
- 6: $\tilde{\mathbf{x}} \leftarrow \tilde{\mathbf{x}}_{i_{\max}}$
- 7: Reconstruct the input signal via Algorithm 1 from $\tilde{\mathbf{x}}$.
- 8: **return** $\tilde{\mathbf{x}}$

reconstruction as it leads the space formed by the intersection of half-spaces (inequality constraints in (25)) to completely shrink to the true value modulo signal $\tilde{\mathbf{x}}$ inside the volume space imposed by unlimited sampling. This volume space is a *cube* because the constraint applied to the modulo samples is $\sup_k |\tilde{x}_k| = \lambda$. Here, the blue planes/lines representing the linear inequalities form a finite-volume space around the optimal point (displayed by the yellow circle inside the cube) by increasing the number of one-bit sampling thresholds. In the top panel, we show the specific case of a trihedron (i.e., modulo samples are $\tilde{\mathbf{x}} \in \mathbb{R}^3$) to represent the effect of increasing the number of threshold sequences on the reconstruction performance.

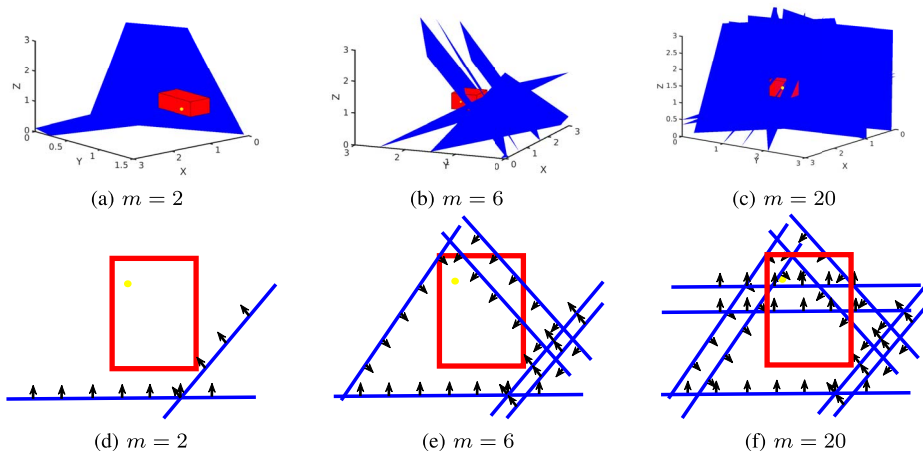


Figure 4. Top: trihedron space (polyhedron (25) in 3 dimensions) (blue), unlimited sampling cube (red), and true value of the modulo signal $\tilde{\mathbf{x}} \in \mathbb{R}^3$ (yellow) for (a) $m = 2$ (b) $m = 6$ and (c) $m = 20$. Bottom: as in the top panel, but only a cross-section (unshaded with same color boundary) at $Z = 0$ plane is shown for (d) $m = 2$ (e) $m = 6$ and (f) $m = 20$. Each inequality constraint is shown by a half-space whose feasible region is marked by black arrows.

The bottom panel shows the same effect for 2-D cross-section of the trihedron. The constraints are not enough to create a finite-volume space in Figure 4(a) and 4(d). On the other hand, in Figure 4(b) and 4(e), such constraints create the desired finite-volume polyhedron space but are unable to capture the optimal point. Finally, in Figure 4(c) and 4(f), the optimal point is successfully captured by the resulting finite-volume space.

V. UNO RECONSTRUCTION: NUMERICAL ILLUSTRATIONS AND ERROR ANALYSES

We assessed the performance of the UNO reconstruction through extensive numerical experiments. In our study, we demonstrate that the size of the cube defined by modulo ADCs (indicated by red contours and shaded regions in Figure 4) and, consequently, the reconstruction error are influenced by the ADC threshold λ . We then investigate the effect of input signal amplitude $\|\mathbf{x}\|_\infty$ on the reconstruction performance. In all experiments, we considered the same high DR input signal as in Section III-D.

A. Varying ADC Threshold

The number of time-varying sampling threshold sequences was set to $m = 400$. In each experiment, the generated signals have the same $\text{DR}_{\mathbf{x}} = 8$ but the ADC threshold λ changes. For a given λ , the sequences of time-varying sampling threshold are drawn randomly following the distributions $\{\tau_{\mathcal{N}}^{(\ell)} \sim \mathcal{N}(\mathbf{0}, \frac{\lambda^2}{9} \mathbf{I})\}_{\ell=1}^m$, and $\{\tau_{\mathcal{U}}^{(\ell)} \sim \mathcal{U}_{[-\lambda, \lambda]}\}_{\ell=1}^m$, respectively. Figure 5 illustrates accurate UNO reconstruction with Gaussian dither for different values of $\lambda \in \{0.2, 0.5, 1\}$. Note that the results of Gaussian and uniform dithering are visually indiscernible and, hence, it suffices to show only one of them (Gaussian) here. Table I compares the reconstruction NMSE (on a \log_{10} scale) of UNO with various dithers, obtained by averaging NSE over 1000 experiments for different values of λ . The uniform dither covers the DR of the modulo samples more effectively than the Gaussian dither. Consequently, the former

provides greater diversity in the bits, resulting in an improved reconstruction. We also observe that increasing in λ leads to higher NMSE because the volume of the unlimited sampling cube grows further, and consequently, more hyperplanes may be required to contain a specific volume around the optimal point in the feasible region.

B. Varying Input Signal Amplitude

Here, we generated the input signals with varying DRs. In each experiment, the ADC threshold λ was fixed to $\lambda = 0.5$, for which we generated sequences of time-varying sampling threshold as $\{\tau_{\mathcal{N}}^{(\ell)} \sim \mathcal{N}(\mathbf{0}, \frac{1}{36} \mathbf{I})\}_{\ell=1}^m$, and $\{\tau_{\mathcal{U}}^{(\ell)} \sim \mathcal{U}_{[-0.5, 0.5]}\}_{\ell=1}^m$, respectively. Figure 6 shows accurate UNO reconstruction with Gaussian dither for different values of $\|\mathbf{x}\|_\infty$. Table II compares the corresponding NMSE of 1000 experiments between UNO with Gaussian and Uniform dithers.

Next, we study the reconstruction for a signal with an extremely high DR, with $\|x(t)\|_\infty = 1000$. In theory, the unlimited sampling theorem guarantees reconstruction with $T \leq \frac{1}{2\Omega_{\max} \epsilon}$. However, in practice, signal reconstruction from unlimited samples has its own limitations due to error propagation by the finite-difference operator. Specifically, for a large DR of input signal compared to that of the ADC threshold λ , the order of difference operator N should also be large. But a large N would also amplify the quantization/round-off noise, leading to an unstable reconstruction. In this scenario, more samples (given by the oversampling factor) are required to decrease N . Note that, unlike conventional ADCs, an abundant number of samples does not lead to an increase in power consumption, manufacturing cost, and per-bit chip area in one-bit ADCs. Figure 6(d) shows an accurate UNO reconstruction for $\lambda = 1$ and a 10.99 times higher sampling rate $1/T$ than the previous experiments.

Although UNO and one-bit $\Sigma\Delta$ method [55] are different in their respective theoretical foundations and applications, here we compare their reconstruction performance for

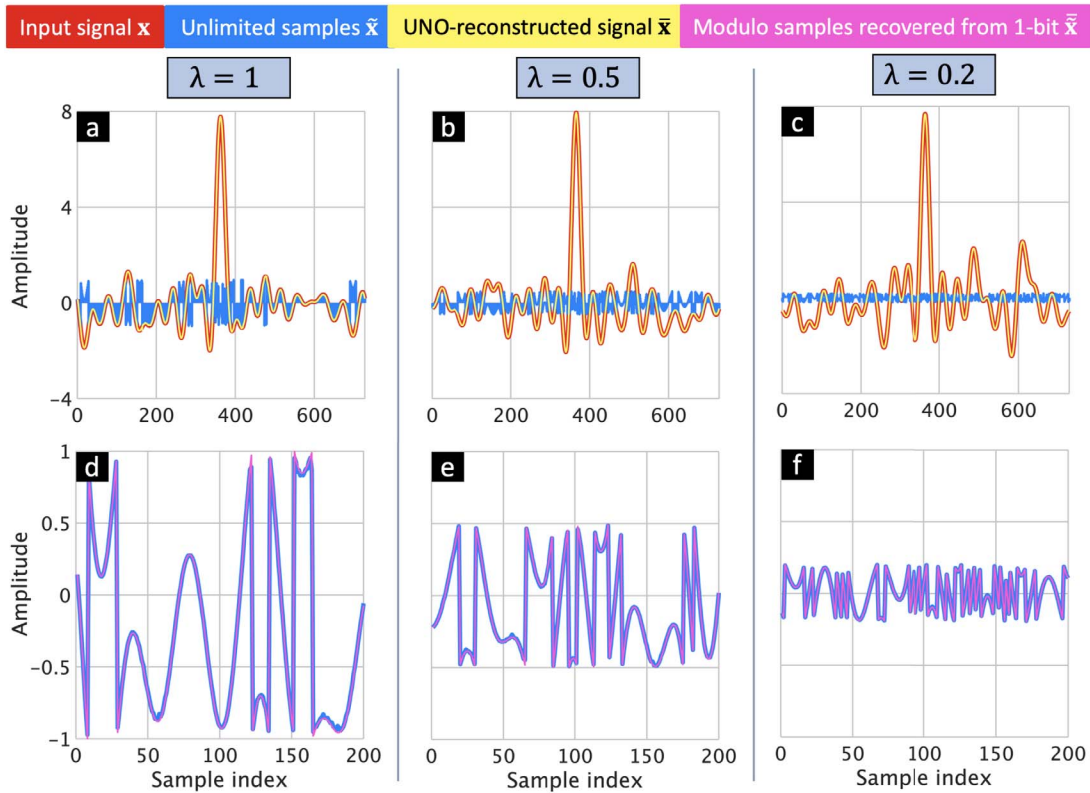


Figure 5. Reconstruction of the input signal from one-bit measurements using UNO when the ADC threshold is (a) $\lambda = 1$, (b) $\lambda = 0.5$, and (c) $\lambda = 0.2$. (d)-(f) As in, respectively, (a)-(c) but the true unlimited samples are compared with their reconstructed samples.

TABLE I
UNO RECONSTRUCTION NMSE FOR FIXED \mathbf{x}

λ	0.2	0.5	1
Gaussian dithered UNO	-72.628	-67.780	-60.987
Uniform dithered UNO	-73.629	-68.470	-61.592

the same signal. The ADC threshold was set to $\lambda = 1$ and sequences of the time-varying sampling threshold were drawn as $\{\tau_{\mathcal{N}}^{(\ell)} \sim \mathcal{N}(\mathbf{0}, \frac{1}{9}\mathbf{I})\}_{\ell=1}^m$ and $\{\tau_{\mathcal{U}}^{(\ell)} \sim \mathcal{U}_{[-1,1]}\}_{\ell=1}^m$, respectively. For the specific case of $\|\mathbf{x}\|_{\infty} = 40$, Figure 7 compares the UNO-reconstructed signal $\bar{\mathbf{x}}$ (with Gaussian dither) with the one-bit unlimited $\Sigma\Delta$ -reconstructed signal $\bar{\mathbf{x}}_{\Sigma\Delta}$ when the ratio between the input signal amplitude and the ADC threshold $\eta = \frac{\|\mathbf{x}\|_{\infty}}{\lambda}$ is large. The one-bit unlimited $\Sigma\Delta$ degenerates in some parts of the input samples, while the UNO accurately reconstruct the signal. Table III further compares the reconstruction NMSE of 1000 experiments, of UNO with Gaussian and Uniform dithers with one-bit unlimited $\Sigma\Delta$ for different amplitudes $\|\mathbf{x}\|_{\infty} \in \{20, 50\}$. Here, the degradation in one-bit $\Sigma\Delta$ reconstruction for large η is because of the round-off noise in software and, primarily, imperfect noise shaping in sigma-delta conversion that results in sample corruption.

Note that the signal dimension is fixed in both UNO and one-bit sigma-delta methods. However, UNO has the flexibility of increasing the total number of one-bit samples by increasing the number of time-varying threshold

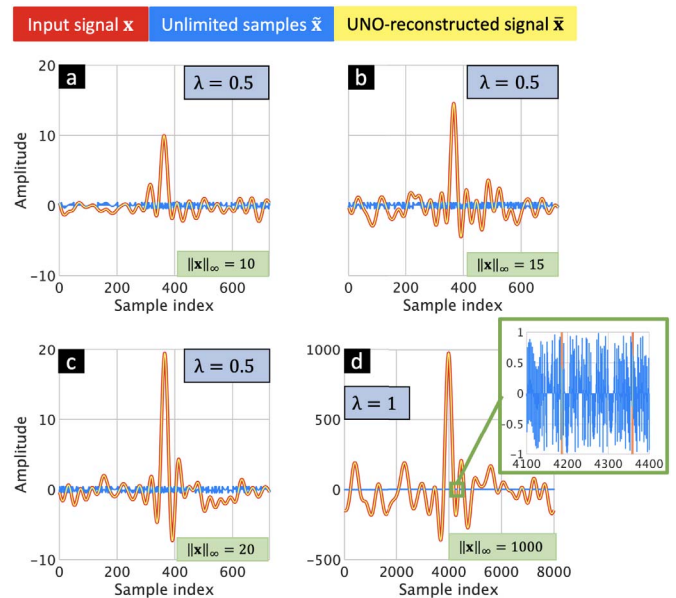


Figure 6. Reconstruction of the input signal from one-bit measurements using UNO Algorithm 2 when the ADC threshold is set to $\lambda = 0.5$ and the input signal amplitude $\|\mathbf{x}\|_{\infty}$ is (a) 10, (b) 15, and (c) 20. (d) As in (a) but for $\lambda = 1$ and $\|\mathbf{x}\|_{\infty} = 1000$. The inset shows the same plot on a larger scale.

sequences. This is not possible with the one-bit $\Sigma\Delta$ quantization, which uses a recursive algorithm to update thresholds, without increasing the signal dimension or

TABLE II
UNO RECONSTRUCTION NMSE FOR $\lambda = 0.5$

$\ \mathbf{x}\ _\infty$	10	15	20
Gaussian dithered UNO	-63.815	-65.728	-63.969
Uniform dithered UNO	-64.125	-65.810	-64.591

TABLE III
RECONSTRUCTION $10 \log_{10}$ NMSE FOR $\lambda = 1$

$\ \mathbf{x}\ _\infty$	One-Bit Unlimited $\Sigma\Delta$	UNO Dither	
		Gaussian	Uniform
20	0.402	-63.261	-64.601
50	3.777	-62.501	-63.159

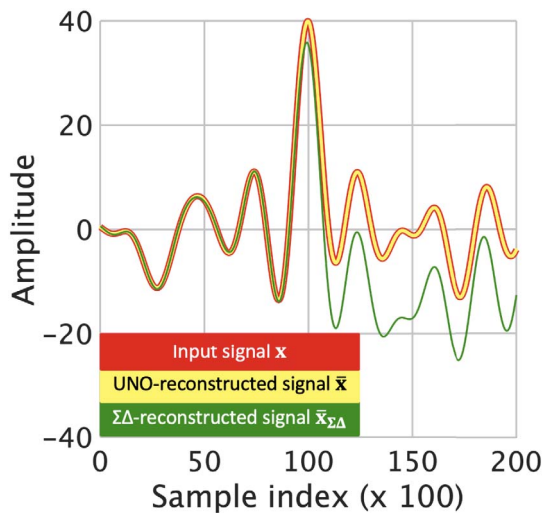


Figure 7. A comparison of reconstruction via UNO and one-bit unlimited $\Sigma\Delta$ when $\lambda = 1$ and $\|\mathbf{x}\|_\infty = 40$.

oversampling factor. The computational complexity of the proposed reconstruction, which comprises RKA and Algorithm 1, is easily obtained as $\mathcal{O}\left(n \ln\left(\frac{1}{\epsilon_1}\right) + 2(N-1)n + \frac{(N-1)}{3}(2N^2 - N - 3)\right)$. It follows that the UNO reconstruction is linearly complex with respect to the signal dimension n .

C. Analysis of Reconstruction Error

To ensure a bounded reconstruction error, the feasible region in (25) cannot have an infinite volume in an asymptotic sense when amplitude constraints are imposed by unlimited sampling. As mentioned before, by introducing more samples, it is possible to obtain a polyhedron with a bounded volume that contains the desired point. Further, as we illustrated in Figure 4, adding more inequality constraints to (25) leads to shrinkage of this polyhedron. We now prove this result, i.e., in a probabilistic sense, that increasing the number of samples leads to the reconstruction error approaching zero, and that the resulting overdetermined linear system of inequalities guarantees the convergence of any consistent reconstruction algorithm which is defined as follows:

Definition 1: Define the modulo signal as $\tilde{\mathbf{x}} = [\tilde{x}_j] \in \mathbb{R}^n$ and the ℓ -th threshold vector by $\boldsymbol{\tau}^{(\ell)} = [\tau_j^{(\ell)}] \in \mathbb{R}^n$ for $\ell \in [m]$. Denote $\tilde{\mathbf{x}} = [\tilde{x}_j] \in \mathbb{R}^n$ as a solution obtained by an arbitrary reconstruction algorithm addressing the feasibility problem (25). Then, such a reconstruction algorithm is said to be consistent when

$$\text{sgn}\left(\tilde{x}_j - \tau_j^{(\ell)}\right) = \text{sgn}\left(\tilde{x}_j - \tau_j^{(\ell)}\right), \quad j \in [n], \ell \in [m]. \quad (26)$$

The concept of consistent reconstruction, as defined in Definition 1, has played a pivotal role in obtaining theoretical guarantees in the field of one-bit compressed sensing [34], [35], [75], [76] and one-bit low-rank matrix sensing [76], [77] as discussed in prior literature. It is important to note that our guarantee is obtained with the uniform assumption of the dithering sequence.

To prove our main theorem, we need to define the following operator:

Definition 2: Define the distance between the modulo signal $\tilde{\mathbf{x}}$ and the j -th hyperplane of (25) as

$$d_j^{(\ell)} = \left| \tilde{x}_j - \tau_j^{(\ell)} \right|, \quad j \in [n], \ell \in [m], \quad (27)$$

where $r_j^{(\ell)} = \text{sgn}\left(\tilde{x}_j - \tau_j^{(\ell)}\right)$. Then, we denote the average of such distances by

$$T_{\text{ave}}(\tilde{\mathbf{x}}) = \frac{1}{mn} \sum_{\ell=1}^m \sum_{j=1}^n d_j^{(\ell)}. \quad (28)$$

Intuitively, it is easy to observe that by reducing the distances between $\tilde{\mathbf{x}}$ and the constraint-associated hyperplanes generally increases the possibility of capturing the desired point. For a specific sample size $m' = mn$, when the volume of the finite space around the desired point is reduced, the mean $\left\{d_j^{(\ell)}\right\}_{j,\ell=1}^{m'}$, i.e., $T_{\text{ave}}(\tilde{\mathbf{x}})$ converges to its mean. In the following lemma, we present the Hoeffding's inequality:

Lemma 3: [74, Theorem 2.2.5] Let $\{X_i\}_{i=1}^n$ be independent, bounded random variables satisfying $X_i \in [a_i, b_i]$, then for any $t > 0$ it holds that

$$\Pr\left(\left|\frac{1}{n} \sum_{i=1}^n (X_i - \mathbb{E}\{X_i\})\right| \geq t\right) \leq 2e^{-\frac{2n^2 t^2}{\sum_{i=1}^n (b_i - a_i)^2}}. \quad (29)$$

We utilize Lemma 3 to provide a concentration inequality in a probability for the finite volume, created by hyperplanes, being contained within the ball around the optimal solution. The following proposition states that the abundant number of samples in conventional one-bit quantization significantly affects the reconstruction performance of any consistent reconstruction algorithm such as RKA addressing a linear feasibility problem in (25):

Proposition 4: Define the set $\mathcal{H} = \{\mathbf{x} \mid \|\mathbf{x}\|_2 \leq \lambda\sqrt{n}\}$. Assume the random threshold follows $\tau \sim \mathcal{U}_{[-\lambda, \lambda]}$. Under the same notations of Definition 2, we have

$$\Pr\left(\sup_{\tilde{\mathbf{x}} \in \mathcal{H}} \left|T_{\text{ave}}(\tilde{\mathbf{x}}) - \frac{\lambda}{2} - \frac{\|\tilde{\mathbf{x}}\|_2^2}{2\lambda n}\right| \geq \epsilon\right) \leq 2e^{-\left(m' \frac{\epsilon^2}{2\lambda^2} - \frac{2n\sqrt{n}\lambda}{\rho}\right)}, \quad (30)$$

where ρ is a positive value.

Proof: For simplicity of notation, denote $d_j^{(\ell)}$ in (27) by $d = |\tilde{x} - \tau|$. Then, we can write

$$\begin{aligned} \mathbb{E}_\tau \{d\} &= \frac{1}{2\lambda} \int_{-\lambda}^{\lambda} |\tilde{x} - \tau| d\tau \\ &= \frac{1}{2\lambda} \left[\int_{-\lambda}^{\tilde{x}} \tilde{x} - \tau d\tau + \int_{\tilde{x}}^{\lambda} \tau - \tilde{x} d\tau \right] = \frac{\lambda}{2} + \frac{\tilde{x}^2}{2\lambda}. \end{aligned} \quad (31)$$

Therefore, we have

$$\mathbb{E}_\tau \{T_{\text{ave}}(\tilde{\mathbf{x}})\} = \frac{1}{mn} \sum_{\ell=1}^m \sum_{j=1}^n \frac{\lambda}{2} + \frac{\tilde{x}_j^2}{2\lambda} = \frac{\lambda}{2} + \frac{\|\tilde{\mathbf{x}}\|_2^2}{2\lambda n}. \quad (32)$$

Note that for each random variable $d_j^{(\ell)}$ we have

$$d_j^{(\ell)} = |\tilde{x}_j - \tau_j^{(\ell)}| \leq |\tilde{x}_j| + |\tau_j^{(\ell)}| \leq 2\lambda. \quad (33)$$

Then, based on the Hoeffding's inequality for bounded random variables presented in Lemma 3, we can write

$$\Pr \left(\left| T_{\text{ave}}(\tilde{\mathbf{x}}) - \frac{\lambda}{2} - \frac{\|\tilde{\mathbf{x}}\|_2^2}{2\lambda n} \right| \geq \epsilon \right) \leq 2e^{-m' \frac{\epsilon^2}{2\lambda^2}}. \quad (34)$$

As we consider the supremum over all $\tilde{\mathbf{x}} \in \mathcal{H}$, it is necessary to multiply the resulting probability by the covering number of the defined set. It can be easily verified that the covering number of ρ -balls required to cover the set \mathcal{H} is upper bounded by

$$\mathcal{N}(\mathcal{H}, \|\cdot\|_2, \rho) \leq \left(1 + \frac{2\lambda\sqrt{n}}{\rho} \right)^n, \quad (35)$$

which can be further upper bounded by

$$\mathcal{N}(\mathcal{H}, \|\cdot\|_2, \rho) \leq e^{n \log(1 + \frac{2\lambda\sqrt{n}}{\rho})} \leq e^{\frac{2\lambda n \sqrt{n}}{\rho}}, \quad (36)$$

which proves the proposition. \blacksquare

Based on this result, the following theorem expresses the universal convergence rate of any consistent reconstruction algorithm in the UNO sampling scheme:

Theorem 2: Under the same assumptions and notations of Definition 2 and Proposition 4, for all $\tilde{\mathbf{x}}, \bar{\mathbf{x}} \in \mathcal{H}$ satisfying the consistent reconstruction property defined in Definition 1, we have

$$\|\tilde{\mathbf{x}} - \bar{\mathbf{x}}\|_2 \leq 4\sqrt{\lambda\epsilon n}, \quad (37)$$

with a probability exceeding $1 - 2e^{-\left(m' \frac{\epsilon^2}{2\lambda^2} - \frac{n}{2} \sqrt{\frac{\lambda}{\epsilon}}\right)}$.

Proof: Define $\tilde{\mathbf{z}} = \frac{1}{2}(\tilde{\mathbf{x}} + \bar{\mathbf{x}})$. We can write $\tilde{z}_j - \tau_j^{(\ell)} = \frac{1}{2}(\tilde{x}_j - \tau_j^{(\ell)} + \bar{x}_j - \tau_j^{(\ell)})$. According to the consistent reconstruction property defined in Definition 1, we can write

$$\left| \tilde{z}_j - \tau_j^{(\ell)} \right| = \frac{1}{2} \left(\left| \tilde{x}_j - \tau_j^{(\ell)} \right| + \left| \bar{x}_j - \tau_j^{(\ell)} \right| \right). \quad (38)$$

Based on (38), for all $j \in [n]$ and $\ell \in [m]$, we can write

$$T_{\text{ave}}(\tilde{\mathbf{z}}) = \frac{1}{2} [T_{\text{ave}}(\tilde{\mathbf{x}}) + T_{\text{ave}}(\bar{\mathbf{x}})]. \quad (39)$$

Following Proposition 4, with a failure probability at most $2e^{-\left(m' \frac{\epsilon^2}{2\lambda^2} - \frac{2n\sqrt{n}\lambda}{\rho}\right)}$, we have

$$\frac{\|\tilde{\mathbf{z}}\|_2^2}{2\lambda n} \geq T_{\text{ave}}(\tilde{\mathbf{z}}) - \frac{\lambda}{2} - \epsilon. \quad (40)$$

Combining the results of (39) and (40) leads to

$$\begin{aligned} \frac{\|\tilde{\mathbf{z}}\|_2^2}{2\lambda n} &\geq \frac{1}{2} [T_{\text{ave}}(\tilde{\mathbf{x}}) + T_{\text{ave}}(\bar{\mathbf{x}})] - \frac{\lambda}{2} - \epsilon \\ &\geq \frac{1}{2} \left[\frac{\lambda}{2} - \epsilon + \frac{\|\tilde{\mathbf{x}}\|_2^2}{2\lambda n} + \frac{\lambda}{2} - \epsilon + \frac{\|\bar{\mathbf{x}}\|_2^2}{2\lambda n} \right] - \frac{\lambda}{2} - \epsilon \\ &= \frac{1}{4\lambda n} (\|\tilde{\mathbf{x}}\|_2^2 + \|\bar{\mathbf{x}}\|_2^2) - 2\epsilon. \end{aligned} \quad (41)$$

Based on the definition of $\tilde{\mathbf{z}}$, we can rewrite (41) in terms of $\tilde{\mathbf{x}}$ and $\bar{\mathbf{x}}$ as follows

$$\|\tilde{\mathbf{x}} + \bar{\mathbf{x}}\|_2^2 \geq 2(\|\tilde{\mathbf{x}}\|_2^2 + \|\bar{\mathbf{x}}\|_2^2) - 16\epsilon\lambda n. \quad (42)$$

By the parallelogram law, we conclude that

$$\|\tilde{\mathbf{x}} - \bar{\mathbf{x}}\|_2^2 = 2(\|\tilde{\mathbf{x}}\|_2^2 + \|\bar{\mathbf{x}}\|_2^2) - \|\tilde{\mathbf{x}} + \bar{\mathbf{x}}\|_2^2, \quad (43)$$

which together with (42) results in

$$\|\tilde{\mathbf{x}} - \bar{\mathbf{x}}\|_2 \leq 4\sqrt{\lambda\epsilon n}. \quad (44)$$

Denote $\rho = 4\sqrt{\lambda\epsilon n}$. Then, according to Proposition 4, with a failure probability at most $2e^{-\left(m' \frac{\epsilon^2}{2\lambda^2} - \frac{n}{2} \sqrt{\frac{\lambda}{\epsilon}}\right)}$, we have $\|\tilde{\mathbf{x}} - \bar{\mathbf{x}}\|_2 \leq \rho$ which completes the proof. \blacksquare

Corollary 1: The decay rate for UNO reconstruction performance concerning m is characterized by $\mathcal{O}\left(m^{-\frac{2}{5}}\right)$.

Proof: To have a decreasing function in $2e^{-\left(m' \frac{\epsilon^2}{2\lambda^2} - \frac{n}{2} \sqrt{\frac{\lambda}{\epsilon}}\right)}$, the number of dithering sequences must meet the following bound: $m \geq \frac{\lambda^2}{\epsilon^2} \sqrt{\frac{\lambda}{\epsilon}}$. The lower bound of m depends on $\epsilon^{-\frac{5}{2}}$, and consequently, the reduction rate of ϵ with respect to m is given by $\mathcal{O}\left(m^{-\frac{2}{5}}\right)$. \blacksquare

Claim 1 shows the significance of UNO sampling.

Claim 1: Increasing the number of time-varying sampling threshold sequences m is not an effective approach to guarantee the desired signal reconstruction with any consistent reconstruction algorithm such as RKA without using modulo sampling.

Proof: To prove this claim, consider $\beta_x \geq \text{DR}_{\mathbf{x}} > \text{DR}_\tau = \lambda$. For simplicity of proof, consider an index $k \in [n]$ such that $x_k = \text{DR}_{\mathbf{x}}$. Also, assume that for an index set $\mathcal{I} = [n] \setminus \{k\}$, we have $\sup_{j \in \mathcal{I}} |x_j| \leq \lambda$. Define the distance between the signal \mathbf{x} and the j -th hyperplane of (6) as

$$d_j^{(\ell)} = \left| x_j - \tau_j^{(\ell)} \right|, \quad j \in [n], \ell \in [m], \quad (45)$$

where $r_j^{(\ell)} = \text{sgn}\left(x_j - \tau_j^{(\ell)}\right)$. We denote the average of such distances by $T_{\text{ave}}(\mathbf{x}) = \frac{1}{mn} \sum_{\ell=1}^m \sum_{j=1}^n d_j^{(\ell)}$. Consider the following lemma:

Lemma 4: Define \mathbf{x}_r as

$$\mathbf{x}_r = [x_1, \dots, x_{k-1}, x_{k+1}, \dots, x_n]^T. \quad (46)$$

Assume the random threshold follows $\tau \sim \mathcal{U}_{[-\lambda, \lambda]}$. Define the set $\mathcal{G} = \{\mathbf{x} \mid \|\mathbf{x}_r\|_2 \leq \lambda\sqrt{n}, x_k = \text{DR}_{\mathbf{x}}\}$ where $\beta_x \geq \text{DR}_{\mathbf{x}} > \lambda$. Then, we have

$$\begin{aligned} \Pr \left(\sup_{\mathbf{x} \in \mathcal{G}} \left| T_{\text{ave}}(\mathbf{x}) - \frac{(n-1)\lambda}{2n} - \frac{\|\mathbf{x}_r\|_2^2}{2\lambda n} - \frac{x_k}{n} \right| \geq \epsilon \right) \\ \leq 2e^{-\left(\frac{2m'\epsilon^2}{(\beta_x + \lambda)^2} - \frac{2n\sqrt{n}\beta_x}{\rho}\right)}, \end{aligned} \quad (47)$$

where ρ is a positive value.

Proof: Rewrite $T_{\text{ave}}(\mathbf{x})$ as

$$T_{\text{ave}}(\mathbf{x}) = \frac{1}{mn} \sum_{\ell=1}^m \sum_{j \in \mathcal{I}} |x_j - \tau_j^{(\ell)}| + \frac{1}{mn} \sum_{\ell=1}^m |x_k - \tau_k^{(\ell)}|. \quad (48)$$

Based on Proposition 4, the expected value of the first term in the right-hand side of (48) can be written as

$$\mathbb{E}_{\tau} \left\{ \frac{1}{mn} \sum_{\ell=1}^m \sum_{j \in \mathcal{I}} |x_j - \tau_j^{(\ell)}| \right\} = \frac{(n-1)\lambda}{2n} + \frac{\|\mathbf{x}_r\|_2^2}{2\lambda n}. \quad (49)$$

It can be easily verified that the expected value of the second term in the right-hand side of (48) is

$$\mathbb{E}_{\tau} \left\{ \frac{1}{mn} \sum_{\ell=1}^m |x_k - \tau_k^{(\ell)}| \right\} = \frac{x_k}{n}. \quad (50)$$

Note that we have

$$\sup_{j \in [n], \ell \in [m]} d_j^{(\ell)} = \beta_x + \lambda. \quad (51)$$

Define the set $\mathcal{D} = \{\mathbf{x} \mid \|\mathbf{x}\|_2 \leq \beta_x \sqrt{n}\}$. Since we have $\mathcal{G} \subseteq \mathcal{D}$, we can write

$$\mathcal{N}(\mathcal{G}, \|\cdot\|_2, \rho) \leq \mathcal{N}(\mathcal{D}, \|\cdot\|_2, \rho) \leq e^{\frac{2\beta_x n \sqrt{n}}{\rho}}. \quad (52)$$

Combining (49)-(52) with Lemma 3 completes the proof of Lemma 4. ■

Define $\mathbf{z} = \frac{1}{2}(\mathbf{x} + \bar{\mathbf{x}})$. We can write $z_j - \tau_j^{(\ell)} = \frac{1}{2}(x_j - \tau_j^{(\ell)} + \bar{x}_j - \tau_j^{(\ell)})$. According to the consistent reconstruction property defined in Definition 1, we can write

$$|z_j - \tau_j^{(\ell)}| = \frac{1}{2} \left(|x_j - \tau_j^{(\ell)}| + |\bar{x}_j - \tau_j^{(\ell)}| \right). \quad (53)$$

Based on (53), for all $j \in [n]$ and $\ell \in [m]$, we can write

$$T_{\text{ave}}(\mathbf{z}) = \frac{1}{2} [T_{\text{ave}}(\mathbf{x}) + T_{\text{ave}}(\bar{\mathbf{x}})]. \quad (54)$$

Based on Lemma 4, with a failure probability at most $2e^{-\left(\frac{2m'\epsilon^2}{(\beta_x + \lambda)^2} - \frac{2n\sqrt{n}\beta_x}{\rho}\right)}$, we have

$$\frac{\|\mathbf{x}_r\|_2^2}{2\lambda n} + \frac{z_k}{n} \geq T_{\text{ave}}(\mathbf{z}) - \frac{(n-1)\lambda}{2n} - \epsilon. \quad (55)$$

Following the proof of Theorem 2, we will obtain

$$\|\mathbf{x}_r + \bar{\mathbf{x}}_r\|_2^2 \geq 2(\|\mathbf{x}_r\|_2^2 + \|\bar{\mathbf{x}}_r\|_2^2) - 16\lambda\epsilon n. \quad (56)$$

By the parallelogram law, we conclude that

$$\|\mathbf{x} - \bar{\mathbf{x}}\|_2^2 \leq 16\lambda\epsilon n + x_k^2 + \bar{x}_k^2 \leq 16\lambda\epsilon n + \beta_x^2 + \lambda^2. \quad (57)$$

Note that for Lemma 4 we set $\rho = \sqrt{16\lambda\epsilon n + \beta_x^2 + \lambda^2}$. Similar to the discussion in Corollary 1, in this case, ϵ decays with the rate $\mathcal{O}(m^{-\frac{2}{5}})$. Therefore, increasing the number of time-varying threshold sequences m leads to decrease in the value of $16\lambda\epsilon n$ in (57). However, the term $\beta_x^2 + \lambda^2$ in (57) does not change with respect to m which implies that the upper recovery bound in (57) cannot be effectively small even by increasing the number of time-varying sampling threshold sequences. ■

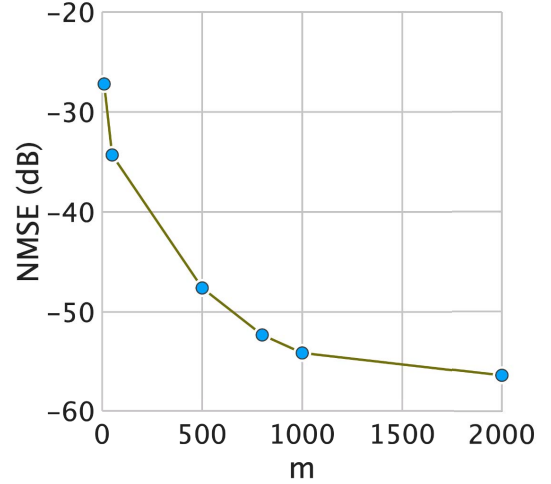


Figure 8. NMSE for RKA-based UNO reconstruction with respect to the number of time-varying threshold sequences m for $\lambda = 0.5$ and $\|\mathbf{x}\|_\infty = 20$.

In Figure 8, we show that UNO reconstruction NMSE of 1000 experiments, significantly improves with the increase in the number of time-varying threshold sequences m . The ADC threshold was set to $\lambda = 0.5$ and the signal DR was $\|\mathbf{x}\|_\infty = 20$. The following theorem summarizes the UNO guarantees:

Theorem 3 (UNO sampling theorem): Assume $x(t)$ to be a finite energy, bandlimited signal with maximum frequency Ω_{\max} with sampling rate $1/T$. Under the assumptions of Theorem 2 and $\epsilon = \frac{\lambda}{256} \left(\frac{2\beta_x}{\lambda}\right)^{-\frac{2}{h}}$ with $h \in \mathbb{N}$, the sufficient condition for the reconstruction of bandlimited signal $x(t)$ from UNO samples, up to additive multiples of 2λ is

$$T \leq \frac{1}{2^h \Omega_{\max} \epsilon}, \quad (58)$$

with a probability higher than $1 - 2e^{-\left(m' \frac{\epsilon^2}{2\lambda^2} - \frac{n}{2} \sqrt{\frac{\lambda}{\epsilon}}\right)}$.

Proof: While reconstructing the modulo samples from one-bit data, the real modulo samples are represented by the linear model

$$\bar{\bar{\mathbf{x}}} = \tilde{\mathbf{x}} + \mathbf{e}. \quad (59)$$

The reconstruction error may be viewed as *noise* for modulo samples. According to [45, Theorem 3], the sampling rate for the *contaminated* modulo samples in (59) to reconstruct the bandlimited signal $x(t)$ to satisfy $\bar{x}_k = x_k + e_k$ is $T \leq \frac{1}{2^h \Omega_{\max} \epsilon}$, where $h \in \mathbb{N}$. It is important to note that the validity of the noisy unlimited sampling theorem [6, Theorem 3] relies on the assumption that the noise added to the modulo samples is almost surely bounded, and

$$\|\mathbf{e}\|_2 \leq \sqrt{n} \frac{\lambda}{4} \left(\frac{2\beta_x}{\lambda}\right)^{-\frac{1}{h}}. \quad (60)$$

where β_x is chosen such that $\beta_x \in 2\lambda\mathbb{Z}$ and $\|\mathbf{x}\|_\infty \leq \beta_x$. As stated in Proposition 4, we have derived the probability of the solution of one-bit signal reconstruction falling within a ball around the optimal solution, as expressed in Theorem 2. When the solution resides within this ball, the norm-2

reconstruction error becomes $\|\tilde{\mathbf{x}} - \bar{\mathbf{x}}\|_2 \leq 4\sqrt{\lambda\epsilon n} = \sqrt{n}\frac{\lambda}{4}$
 $\left(\frac{2\beta_x}{\lambda}\right)^{-\frac{1}{h}}$ in a probability, which implies $\epsilon = \frac{\lambda}{256} \left(\frac{2\beta_x}{\lambda}\right)^{-\frac{2}{h}}$. ■

Theorem 3 states that the upper bound on T for UNO sampling is lower than or equal to that of the unlimited sampling (the equality holds when $h = 1$) which associates with a higher sampling rate in UNO. As mentioned earlier, oversampling is a common scenario in one-bit quantization techniques and is not a major concern in UNO implementation. Moreover, the corresponding reconstructed modulo samples in UNO obey $|\tilde{x}_k| < \lambda$. This ensures that N in (22) guarantees $\Delta^N \bar{\mathbf{x}} \equiv \mathcal{M}_\lambda(\Delta^N \bar{\mathbf{x}})$ or equivalently $\Delta^N \bar{\mathbf{x}} \equiv \mathcal{M}_\lambda(\Delta^N \tilde{\mathbf{x}})$; we refer the reader to [6] for more details on this aspect. As a result, UNO reconstructs the input samples x_k in the sense that $\tilde{x}_k = x_k + e_k$ (up to additive multiples of 2λ) with the same N considered in the noiseless unlimited sampling reconstruction of [45, Section IV.B].

VI. RECONSTRUCTION IN THE PRESENCE OF NOISE

Previously, for modulo sampling, [6] has shown recovery of noisy bandlimited samples from their modulo samples up to an unknown additive constant, where the noise is entry-wise additive to the modulo samples, i.e., $\tilde{\mathbf{y}} = \tilde{\mathbf{x}} + \epsilon$, and ϵ is the noise vector. Contrary to this, we propose an approach to reconstruct UNO sampled signal when the noise is additive to the input signal, which itself has a linear relationship with a desired parameter. This linear model for the noisy measurement \mathbf{y} is

$$\mathbf{y} = \mathbf{x} + \epsilon, \quad \mathbf{x} = \mathbf{A}\boldsymbol{\theta}, \quad \mathbf{A} \in \mathbb{R}^{r \times s}, \quad (61)$$

where $\boldsymbol{\theta}$ is the desired parameter vector and the noise follows the distribution $\epsilon \sim \mathcal{N}(0, \sigma_\epsilon^2 \mathbf{I}_m)$. Here, we may have $\mathbf{y} \notin [-\lambda, \lambda]$. Our goal is to estimate $\boldsymbol{\theta}$ from the UNO samples of noisy measurement \mathbf{y} obtained as

$$\mathbf{r}^{(\ell)} = \text{sgn}(\mathcal{M}_\lambda(\mathbf{y}) - \boldsymbol{\tau}^{(\ell)}), \quad \ell \in [m]. \quad (62)$$

Our recovery approach comprises using RKA and Algorithm 1 (with N specified by (55)) to reconstruct noisy measurements from one-bit data, and then exploiting the PnP-ADMM method to estimate the desired parameters from linear overdetermined or undetermined systems.

A. PnP-ADMM-Based UNO Reconstruction

From the UNO samples (62), we reconstruct \mathbf{y} via Algorithm 2. The reconstructed signal $\bar{\mathbf{y}}$ also follows the linear model (61). Therefore, we use $\bar{\mathbf{y}}$ to estimate $\boldsymbol{\theta}$ through the regularization

$$\hat{\boldsymbol{\theta}} = \arg \min_{\boldsymbol{\theta}} \|\bar{\mathbf{y}} - \mathbf{A}\boldsymbol{\theta}\|_2^2 + \eta\rho(\boldsymbol{\theta}), \quad (63)$$

where $\rho(\boldsymbol{\theta})$ is the penalty term and $\eta > 0$ is the real-valued regularization parameter. There is a rich body of literature to select the penalty function $\rho(\cdot)$ including the ℓ_1 -norm [78], smoothly clipped absolute deviation (SCAD) [79], adaptive least absolute shrinkage and selection operator (LASSO) [80]

Algorithm 3 Noisy UNO algorithm.

Input: Sequences of one-bit measurements $\{\mathbf{r}^{(\ell)} = \text{sgn}(\mathcal{M}_\lambda(\mathbf{y}) - \boldsymbol{\tau}^{(\ell)})\}_{\ell=1}^m$, where \mathbf{y} follows (61), $\boldsymbol{\tau}_{\mathcal{N}}^{(\ell)} \sim \mathcal{N}(\mathbf{0}, \sigma_{\boldsymbol{\tau}}^2 \mathbf{I})$ (for Gaussian dithering), $\boldsymbol{\tau}_{\mathcal{U}}^{(\ell)} \sim \mathcal{U}_{[-a, a]}$ (for Uniform dithering), ADC threshold λ , design parameters η and β , total number of iterations k_{\max} .

Output: The reconstruction of the parameter of interest $\hat{\boldsymbol{\theta}}$.

- 1: $\sigma_{\boldsymbol{\tau}} \leftarrow \frac{\lambda}{\sqrt{2 \ln(\frac{2m}{\eta})}} \triangleright$ For Gaussian dithering.
- 2: $a \leftarrow \lambda \triangleright$ For Uniform dithering.
- 3: Reconstruct modulo samples from RKA.
- 4: Reconstruct $\bar{\mathbf{y}}$ from $\bar{\mathbf{y}}$ with Algorithm 1.
- 5: **for** $k = 1 : k_{\max}$ **do**
- 6: $\boldsymbol{\theta}_k \leftarrow \min_{\boldsymbol{\theta}} \left\{ \|\bar{\mathbf{y}} - \mathbf{A}\boldsymbol{\theta}\|_2^2 + \frac{\beta}{2} \|\boldsymbol{\theta} - \boldsymbol{\nu}_{k-1} + \mathbf{u}_{k-1}\|^2 \right\}$.
- 7: $\boldsymbol{\nu}_k \leftarrow \mathcal{D}(\boldsymbol{\theta}_k + \mathbf{u}_{k-1})$.
- 8: $\mathbf{u}_k \leftarrow \mathbf{u}_{k-1} + \boldsymbol{\theta}_k - \boldsymbol{\nu}_k$.
- 9: **return** $\hat{\boldsymbol{\theta}} \leftarrow \boldsymbol{\theta}_{k_{\max}}$.

and the minimax-concave (MC) penalty which has a relationship with Huber functions [81].

One of the standard approaches to solve regularized problems such as in (63) is ADMM that relies on splitting variables [82]. We consider

$$\hat{\boldsymbol{\theta}} = \arg \min_{\boldsymbol{\theta}} \|\bar{\mathbf{y}} - \mathbf{A}\boldsymbol{\theta}\|_2^2 + \eta\rho(\boldsymbol{\nu}) \text{ subject to } \boldsymbol{\theta} = \boldsymbol{\nu}. \quad (64)$$

Using the augmented Lagrangian, we reformulate problem (64) as

$$\begin{aligned} & \text{minimize} \max_{\boldsymbol{\theta}, \boldsymbol{\nu}} \mathbf{p} \\ & \times \left\{ \|\bar{\mathbf{y}} - \mathbf{A}\boldsymbol{\theta}\|_2^2 + \eta\rho(\boldsymbol{\nu}) + \mathbf{p}^\top(\boldsymbol{\theta} - \boldsymbol{\nu}) + \frac{\beta}{2} \|\boldsymbol{\theta} - \boldsymbol{\nu}\|^2 \right\}, \end{aligned} \quad (65)$$

where \mathbf{p} is the dual variable and β is a real-valued design parameter. Denote $\mathbf{u} = \frac{\mathbf{p}}{\beta}$. Then,

$$\begin{aligned} & \text{minimize} \max_{\boldsymbol{\theta}, \boldsymbol{\nu}} \mathbf{u} \\ & \times \left\{ \|\bar{\mathbf{y}} - \mathbf{A}\boldsymbol{\theta}\|_2^2 + \eta\rho(\boldsymbol{\nu}) + \frac{\beta}{2} \|\boldsymbol{\theta} - \boldsymbol{\nu} + \mathbf{u}\|^2 - \frac{\beta}{2} \|\mathbf{u}\|^2 \right\}. \end{aligned} \quad (66)$$

The ADMM tackles (66) by alternating the minimization of $\boldsymbol{\theta}$ and $\boldsymbol{\nu}$. The update of $\boldsymbol{\nu}$ is essentially denoising of $\boldsymbol{\theta}_k + \mathbf{u}_{k-1}$ by the regularization $\eta\rho(\boldsymbol{\nu})$. This is the key idea behind PnP-ADMM, where the proximal projection

$$\boldsymbol{\nu}_k = \arg \min_{\boldsymbol{\nu}} \left\{ \eta\rho(\boldsymbol{\nu}) + \frac{\beta}{2} \|\boldsymbol{\nu} - \boldsymbol{\theta}_k - \mathbf{u}_{k-1}\|^2 \right\} \quad (67)$$

is replaced with an appropriate denoiser $\mathcal{D}(\cdot)$. For further details on various denoisers used in PnP techniques, we refer the interested reader to [63]. Algorithm 3 summarizes the noisy UNO reconstruction procedure. It is worth noting that when the

sampling matrix \mathbf{A} is set to the identity matrix, the initial step of the signal reconstruction algorithm in the ADMM component is eliminated, resulting in a straightforward denoising process using the PnP framework.

B. ADC Threshold Selection in Noisy UNO

Theorem 4 certifies that the additive noise to the input signal results in an additive noise in modulo domain.

Theorem 4: Assume the noise vector in the measurement model $\mathbf{y} = \mathbf{x} + \mathbf{z}$ to be $\mathbf{z} = [z_k] \sim \mathcal{N}(0, \sigma_z^2 \mathbf{I}_m)$. Denote $\tilde{\mathbf{x}} = \mathcal{M}_\lambda(\mathbf{x})$ and $\tilde{\mathbf{z}} = [\tilde{z}_k]$, $\tilde{z}_k = \text{mod}(z_k, 2\lambda) - 2(1 - q_k)\lambda$, $q_k \in \{0, 1\}$. Then, $\tilde{\mathbf{y}} = \tilde{\mathbf{x}} + \tilde{\mathbf{z}}$, where $\tilde{\mathbf{y}} = \mathcal{M}_\lambda(\mathbf{y})$.

Proof: Applying the modulo operator \mathcal{M}_λ in (18) to the noisy measurements \mathbf{y} produces

$$\tilde{\mathbf{y}} = \mathcal{M}_\lambda(\mathbf{y}) = \mathcal{M}_\lambda(\mathbf{x} + \mathbf{z}) = \mathbf{x} + \mathbf{z} - 2\lambda \left\lfloor \frac{\mathbf{x}}{2\lambda} + \frac{1}{2} + \frac{\mathbf{z}}{2\lambda} \right\rfloor, \quad (68)$$

where $\mathbf{z} \sim \mathcal{N}(0, \sigma_z^2 \mathbf{I}_m)$. Since we have $\lfloor a + b \rfloor \geq \lfloor a \rfloor + \lfloor b \rfloor$ for two arbitrary real numbers a and b , it follows from (68) that

$$\begin{aligned} \mathcal{M}_\lambda(\mathbf{x} + \mathbf{z}) &= \mathbf{x} + \mathbf{z} - 2\lambda \left\lfloor \frac{\mathbf{x}}{2\lambda} + \frac{1}{2} + \frac{\mathbf{z}}{2\lambda} \right\rfloor \\ &\leq \mathbf{x} - 2\lambda \left\lfloor \frac{\mathbf{x}}{2\lambda} + \frac{1}{2} \right\rfloor + \mathbf{z} - 2\lambda \left\lfloor \frac{\mathbf{z}}{2\lambda} \right\rfloor \\ &= \tilde{\mathbf{x}} + \mathbf{z} - 2\lambda \left\lfloor \frac{\mathbf{z}}{2\lambda} \right\rfloor = \tilde{\mathbf{x}} + \text{mod}(\mathbf{z}, 2\lambda). \end{aligned} \quad (69)$$

Using the identity $\lfloor a + b \rfloor \leq \lfloor a \rfloor + \lfloor b \rfloor + 1$, we obtain

$$\mathcal{M}_\lambda(\mathbf{x} + \mathbf{z}) \geq \tilde{\mathbf{x}} + \text{mod}(\mathbf{z}, 2\lambda) - 2\lambda. \quad (70)$$

A binary combination of the right-hand sides of (69) and (70) is equivalent to $\mathcal{M}_\lambda(x_k + z_k)$, i.e.,

$$\begin{aligned} \tilde{y}_k &= \mathcal{M}_\lambda(x_k + z_k) \\ &= q_k (\tilde{x}_k + \text{mod}(z_k, 2\lambda)) \\ &\quad + (1 - q_k) (\tilde{x}_k + \text{mod}(z_k, 2\lambda) - 2\lambda), \\ &= \tilde{x}_k + \text{mod}(z_k, 2\lambda) - 2(1 - q_k)\lambda, \end{aligned} \quad (71)$$

where $q_k \in \{0, 1\}$. Rewrite (71) as $\tilde{y}_k = \tilde{x}_k + \tilde{z}_k$, where $\tilde{z}_k = \text{mod}(z_k, 2\lambda) - 2(1 - q_k)\lambda$, which completes the proof. ■

It follows from Theorem 4 that the noise corruption in the input signal carries over to the modulo samples. The following theorem unveils the UNO reconstruction guarantee in the presence of noise.

Theorem 5: (UNO sampling with noise) Under the assumptions of Theorems 2 and 4, consider $\epsilon = \left(\frac{\sqrt{\lambda}}{16} \left(\frac{2\beta_x}{\lambda}\right)^{-\frac{1}{h}} - \frac{\lfloor 2q_k\lambda - 1 \rfloor}{4\sqrt{\lambda}}\right)^2$ with $h \in \mathbb{N}$. Then, the sufficient condition to reconstruct bandlimited signal $x(t)$ from corrupted UNO samples $\tilde{\mathbf{y}}$, up to additive multiples of 2λ is

$$T \leq \frac{1}{2^h \Omega_{\max} e}, \quad (72)$$

with a probability exceeding $1 - 2e^{-\left(m' \frac{\epsilon^2}{2\lambda^2} - \frac{n}{2} \sqrt{\frac{\epsilon}{\lambda}}\right)}$.

Proof: The proof follows from repeating the proof of Theorem 3 by replacing the recovery error \mathbf{e} with $\tilde{\mathbf{z}} + \mathbf{e}$. As previously mentioned, the validity of the noisy unlimited sampling theorem [6] relies on the assumption that the noise added to the modulo samples remains bounded. In our case, the additive noise to the modulo samples is given by $\tilde{\mathbf{z}} + \mathbf{e}$, where $\tilde{z}_k = \text{mod}(z_k, 2\lambda) - 2(1 - q_k)\lambda$. The error of one-bit signal recovery is bounded by $4\sqrt{\lambda\epsilon n}$ with a probability of at least defined in Proposition 4. Additionally, the noise $\tilde{\mathbf{z}}$ is bounded by $|\tilde{z}_k| \leq |2q_k\lambda - 1|$ (which follows from the fact that $\text{mod}(z_k, 2\lambda) \leq 2\lambda - 1$). Furthermore, we derive the inequality $\|\tilde{\mathbf{z}} + \mathbf{e}\|_2 \leq \|\tilde{\mathbf{z}}\|_2 + \|\mathbf{e}\|_2 \leq \sqrt{n} |2q_k\lambda - 1| + 4\sqrt{\lambda\epsilon n} = \sqrt{n} \frac{\lambda}{4} \left(\frac{2\beta_x}{\lambda}\right)^{-\frac{1}{h}}$, which completes the proof. ■

The aforementioned theorem states that as the noise level increases, more one-bit samples are required to have a good reconstruction. This is similar to other conventional noisy samplers. For example, Cadzow denoising [83], used to suppress the effect of noise in sparse samplers similarly requires such an oversampling [84].

C. Numerical Examples

We investigated PnP-ADMM-based noisy UNO reconstruction with $\mathbf{A} = [a_{ij}]$ to be $a_{ij} \sim \mathcal{N}(0, 1)$ and $\mathbf{y} = \mathbf{y}_t + \epsilon$, where \mathbf{y}_t was generated as in Section III-D and $\epsilon \sim \mathcal{N}(\mathbf{0}, \sigma_\epsilon^2 \mathbf{I}_m)$. Figure 9(a) and 9(b) show accurate noisy UNO reconstruction of the parameter vector with fixed $\sigma_\epsilon^2 = 0.1$ in case of, respectively, overdetermined ($r = 728, s = 100$) and underdetermined ($r = 728, s = 1000$) systems in (61). Figure 9(c) demonstrates the efficacy of Noisy UNO in estimating the desired parameter θ from (61) when only UNO samples of noisy measurement \mathbf{y} are available.

Table IV and V report the reconstruction NMSE of θ , i.e., averaged version of $\text{NSE}_\theta \triangleq \frac{\|\theta - \hat{\theta}\|_2^2}{\|\theta\|_2^2}$, over 1000 experiments for different noise variances $\sigma_\epsilon^2 \in \{0.01, 0.05, 0.1\}$ using the PnP-ADMM-based UNO with Gaussian and Uniform dithers, respectively. Here, following Theorem 5, the ADC threshold was set to $\lambda = 1.5$.

Next, to be consistent with the results in [30], [68], we consider sampling a sinusoidal: $x_n(t) = A \cos(2\pi f_0 t) + n(t)$, where $A = 16$, $f_0 = 2$, $T = 0.0005$, and $n(t)$ is Gaussian noise with standard deviation $\sigma_n = 0.5$. Note that we set the ADC threshold $\lambda = 2$. Figure 10 shows successful reconstruction with UNO under this noisy setting. We estimate the parameter vector $\theta = [A, f_0]^T$ of the input signal by setting the sampling matrix \mathbf{A} in PnP-ADMM to be the DFT matrix. Table VI shows that the NMSEs in the estimate $\hat{\theta} = [\hat{A}, \hat{f}_0]^T$ obtained by PnP-UNO reconstruction of 1000 experiments are negligible.

VII. DISCUSSION

The design of alternative sampling schemes to enable practical implementations of Shannon's theorem – from theory to praxis – has been an active research topic for decades. In this context, our proposed UNO presents a framework of merging one-bit quantization and unlimited sampling.

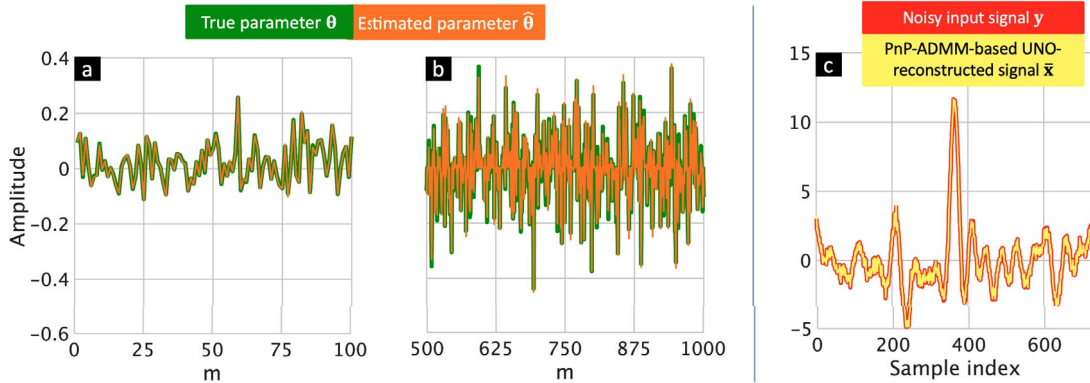


Figure 9. Reconstruction of the desired parameter vector θ following the linear model (61) using PnP-ADMM-based UNO for an (a) overdetermined system with $\mathbf{A} \in \mathbb{R}^{728 \times 100}$ and (b) underdetermined system with $\mathbf{A} \in \mathbb{R}^{728 \times 1000}$. Here, to facilitate a better visual presentation, the number of threshold sequences start from $m = 500$. (c) Reconstruction of the noisy input signal from one-bit measurements using PnP-ADMM-based UNO.

TABLE IV
RECONSTRUCTION $10 \log_{10} \text{NMSE}_{\theta}$ WITH PnP-ADMM NOISY UNO (WITH GAUSSIAN DITHERING)

σ_{ϵ}^2	Overdetermined System	Underdetermined System
0.1	-48.294	-38.128
0.05	-52.676	-42.347
0.01	-56.815	-45.259

TABLE V
RECONSTRUCTION $10 \log_{10} \text{NMSE}_{\theta}$ WITH PnP-ADMM NOISY UNO (WITH UNIFORM DITHERING)

σ_{ϵ}^2	Overdetermined System	Underdetermined System
0.1	-48.304	-39.024
0.05	-53.506	-44.148
0.01	-56.919	-46.191

TABLE VI
SINUSOID PARAMETER ESTIMATION
 $10 \log_{10} \text{NMSE}$

σ_n	$\frac{ \bar{f}_0 - f_0 ^2}{ f_0 ^2}$	$\frac{ \bar{A} - A ^2}{ A ^2}$
0.5	-35.152	-36.437

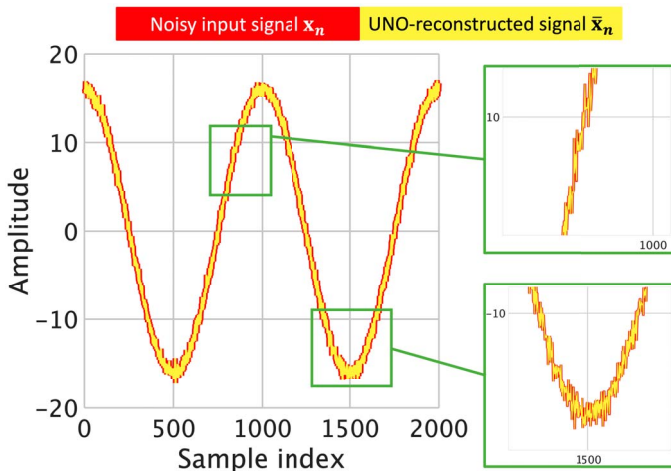


Figure 10. The original discrete noisy sinusoidal vector \mathbf{x}_n and its UNO reconstruction $\bar{\mathbf{x}}_n$. In this comparison the ADC threshold was set to $\lambda = 2$.

This sampling framework naturally facilitates a judicious design of time-varying sampling thresholds by properly utilizing the information on the distance between the signal values and the thresholds in a high DR regime. The noiseless

UNO reconstruction relies on exploiting RKA algorithm while the noisy reconstruction is based on the PnP-ADMM heuristic. These low-complexity approaches are preferable over existing costly reconstruction optimization approaches [63], [64].

The UNO framework achieves multiple objectives of high sampling rate, unlimited DR, less complex and potentially low-power implementations. Our numerical and theoretical analyses demonstrate accurate reconstruction for several different scenarios. Some theoretical questions remain open, e.g. on the relationship between the number of threshold sequences m and reconstruction error in a closed form. This may help in finding the required number of threshold sequences for perfect reconstruction. The single-stage or direct reconstruction from one-bit samples, without unfolding or additional processing, remains an interesting open problem. Further, a hardware verification of UNO on the lines of unlimited sampling in [45] is also desirable.

Acknowledgment

The authors are grateful to Prof. Ayush Bhandari of Imperial College, London for helpful discussions related to his work in [55] and for providing the relevant source codes to facilitate meaningful comparison.

REFERENCES

- [1] A. J. Jerri, "The Shannon sampling theorem—Its various extensions and applications: A tutorial review," *Proc. IEEE*, vol. 65, no. 11, pp. 1565–1596, Nov. 1977.
- [2] J. H. Van Vleck and D. Middleton, "The spectrum of clipped noise," *Proc. IEEE*, vol. 54, no. 1, pp. 2–19, Jan. 1966.
- [3] J. S. Abel, "Restoring a clipped signal," in *Proc. IEEE Int. Conf. Acoust., Speech, Signal Process.*, 1991, pp. 1745–1748.
- [4] S. Ting and A. H. Sayed, "Mitigation of clipping in sensors," in *Proc. IEEE Int. Conf. Acoust., Speech Signal Process.*, 2013, pp. 5934–5938.

- [5] A. Adler, V. Emiya, M. G. Jafari, M. Elad, R. Gribonval, and M. Plumbley, "Audio inpainting," *IEEE Trans. Audio, Speech, Lang. Process.*, vol. 20, no. 3, pp. 922–932, Mar. 2012.
- [6] A. Bhandari, F. Kraher, and R. Raskar, "On unlimited sampling and reconstruction," *IEEE Trans. Signal Process.*, vol. 69, pp. 3827–3839, 2020.
- [7] F. Esqueda, S. Bilbao, and V. Välimäki, "Aliasing reduction in clipped signals," *IEEE Trans. Signal Process.*, vol. 64, no. 20, pp. 5255–5267, Oct. 2016.
- [8] V. Gregers-Hansen, S. M. Brockett, and P. E. Cahill, "A stacked A-to-D converter for increased radar signal processor dynamic range," in *Proc. IEEE Radar Conf.*, 2001, pp. 169–174.
- [9] D. Prasanna, C. R. Murthy, and C. Sriram, "On the application of modulo-ADCs for compressed sensing," in *Proc. Asilomar Conf. Signals, Syst., Comput.*, 2021, pp. 852–856.
- [10] A. Bhandari, F. Kraher, and R. Raskar, "On unlimited sampling," in *Proc. IEEE Int. Conf. Sampling Theory Appl.*, 2017, pp. 31–35.
- [11] S. Rudresh, A. Adiga, B. Shenoy, and C. S. Seelamantula, "Wavelet-based reconstruction for unlimited sampling," in *Proc. IEEE Int. Conf. Acoust., Speech Signal Process.*, 2018, pp. 4584–4588.
- [12] A. Bhandari, "Unlimited sampling with sparse outliers: Experiments with impulsive and jump or reset noise," in *Proc. IEEE Int. Conf. Acoust., Speech Signal Process.*, 2022, pp. 5403–5407.
- [13] Y. Xiao, L. Huang, D. Ramírez, C. Qian, and H. So, "Covariance matrix recovery from one-bit data with non-zero quantization thresholds: Algorithm and performance analysis," *IEEE Trans. Signal Process.*, vol. 71, pp. 4060–4076, 2023.
- [14] D. K. W. Ho and B. D. Rao, "Antithetic dithered 1-bit massive MIMO architecture: Efficient channel estimation via parameter expansion and PML," *IEEE Trans. Signal Process.*, vol. 67, no. 9, pp. 2291–2303, May 2019.
- [15] T. Kugelstadt, "Active filter design techniques," in *Op Amps for Everyone Literature Number SLOD006A*, R. Mancini, Ed., Burlington, MA, USA: Elsevier, 2002.
- [16] A. Mezghani and A. Swindlehurst, "Blind estimation of sparse broadband massive MIMO channels with ideal and one-bit ADCs," *IEEE Trans. Signal Process.*, vol. 66, no. 11, pp. 2972–2983, Jun. 2018.
- [17] A. Eamaz, F. Yeganegi, and M. Soltanalian, "Modified arcsine law for one-bit sampled stationary signals with time-varying thresholds," in *Proc. IEEE Int. Conf. Acoust., Speech Signal Process.*, 2021, pp. 5459–5463.
- [18] T. Yang, J. Maly, S. Dirksen, and G. Caire, "Plug-in channel estimation with dithered quantized signals in spatially non-stationary massive MIMO systems," *IEEE Trans. Commun.*, vol. 72, no. 1, pp. 387–402, Jan. 2024.
- [19] C. Kong, A. Mezghani, C. Zhong, A. Swindlehurst, and Z. Zhang, "Multipair massive MIMO relaying systems with one-bit ADCs and DACs," *IEEE Trans. Signal Process.*, vol. 66, no. 11, pp. 2984–2997, Jun. 2018.
- [20] Y. Li, C. Tao, G. Seco-Granados, A. Mezghani, A. Swindlehurst, and L. Liu, "Channel estimation and performance analysis of one-bit massive MIMO systems," *IEEE Trans. Signal Process.*, vol. 65, no. 15, pp. 4075–4089, Aug. 2017.
- [21] C.-L. Liu and P. Vaidyanathan, "One-bit sparse array DoA estimation," in *Proc. IEEE Int. Conf. Acoust., Speech Signal Process.*, 2017, pp. 3126–3130.
- [22] C. Güntürk, "One-bit sigma-delta quantization with exponential accuracy," *Commun. Pure Appl. Math.*, vol. 56, no. 11, pp. 1608–1630, 2003.
- [23] P. Deift, F. Kraher, and C. S. Güntürk, "An optimal family of exponentially accurate one-bit sigma-delta quantization schemes," *Commun. Pure Appl. Math.*, vol. 64, no. 7, pp. 883–919, 2011.
- [24] C. Qian and J. Li, "ADMM for harmonic retrieval from one-bit sampling with time-varying thresholds," in *Proc. IEEE Int. Conf. Acoust., Speech Signal Process.*, 2017, pp. 3699–3703.
- [25] C. Gianelli, L. Xu, J. Li, and P. Stoica, "One-bit compressive sampling with time-varying thresholds for sparse parameter estimation," in *Proc. IEEE Sensor Array Multichannel Signal Process. Workshop*, 2016, pp. 1–5.
- [26] A. Eamaz, F. Yeganegi, and M. Soltanalian, "One-bit phase retrieval: More samples means less complexity?" *IEEE Trans. Signal Process.*, vol. 70, pp. 4618–4632, 2022.
- [27] A. Eamaz, F. Yeganegi, and M. Soltanalian, "Covariance recovery for one-bit sampled non-stationary signals with time-varying sampling thresholds," *IEEE Trans. Signal Process.*, vol. 70, pp. 5222–5236, 2022.
- [28] A. Eamaz, F. Yeganegi, and M. Soltanalian, "Covariance recovery for one-bit sampled stationary signals with time-varying sampling thresholds," *Signal Process.*, vol. 206, 2023, Art. no. 108899.
- [29] P. Wang, J. Li, M. Pajovic, P. T. Boufounos, and P. V. Orlik, "On angular-domain channel estimation for one-bit massive MIMO systems with fixed and time-varying thresholds," in *Proc. Asilomar Conf. Signals, Syst., Comput.*, 2017, pp. 1056–1060.
- [30] F. Xi, Y. Xiang, S. Chen, and A. Nehorai, "Gridless parameter estimation for one-bit MIMO radar with time-varying thresholds," *IEEE Trans. Signal Process.*, vol. 68, pp. 1048–1063, 2020.
- [31] I. Robinson, J. Toplicar, and J. Heston, Analog to digital conversion using differential dither. (2019, May 21). US Patent 10,298,256.
- [32] A. Ali and P. Gulati, Background calibration of reference, DAC, and quantization non-linearity in ADCs. (2020, Jan. 28). US Patent 10,547,319.
- [33] C. Thrampoulidis and A. S. Rawat, "The generalized LASSO for sub-Gaussian measurements with dithered quantization," *IEEE Trans. Inf. Theory*, vol. 66, no. 4, pp. 2487–2500, Apr. 2020.
- [34] R. Baraniuk, S. Foucart, D. Needell, Y. Plan, and M. Wootters, "Exponential decay of reconstruction error from binary measurements of sparse signals," *IEEE Trans. Inf. Theory*, vol. 63, no. 6, pp. 3368–3385, Jun. 2017.
- [35] C. Xu and L. Jacques, "Quantized compressive sensing with RIP matrices: The benefit of dithering," *Inf. Inference: A J. IMA*, vol. 9, no. 3, pp. 543–586, 2020.
- [36] E. Romanov and O. Ordentlich, "Above the Nyquist rate, modulo folding does not hurt," *IEEE Signal Process. Lett.*, vol. 26, no. 8, pp. 1167–1171, Aug. 2019.
- [37] A. Bhandari and F. Kraher, "On identifiability in unlimited sampling," in *Proc. IEEE Int. Conf. Sampling Theory Appl.*, 2019, pp. 1–4.
- [38] A. Weiss, E. Huang, O. Ordentlich, and G. Wornell, "Blind modulo analog-to-digital conversion," *IEEE Trans. Signal Process.*, vol. 70, pp. 4586–4601, 2022.
- [39] A. Bhandari, F. Kraher, and R. Raskar, "Unlimited sampling of sparse signals," in *Proc. IEEE Int. Conf. Acoust., Speech Signal Process.*, 2018, pp. 4569–4573.
- [40] F. Ji, P. Pratibha, and W. P. Tay, "On folded graph signals," in *Proc. IEEE Global Conf. Signal Inf. Process.*, 2019, pp. 1–5.
- [41] S. Fernández-Menduina, F. Kraher, G. Leus, and A. Bhandari, "DoA estimation via unlimited sensing," in *Proc. Eur. Signal Process. Conf.*, 2021, pp. 1866–1870.
- [42] Z. Liu, A. Bhandari, and B. Clerckx, " λ -MIMO: Massive MIMO via modulo sampling," *IEEE Trans. Commun.*, vol. 71, no. 11, pp. 6301–6315, Nov. 2023.
- [43] O. Musa, P. Jung, and N. Goertz, "Generalized approximate message passing for unlimited sampling of sparse signals," in *Proc. IEEE Global Conf. Signal Inf. Process.*, 2018, pp. 336–340.
- [44] D. Florescu and A. Bhandari, "Unlimited sampling with local averages," in *Proc. IEEE Int. Conf. Acoust., Speech Signal Process.*, 2022, pp. 5742–5746.
- [45] A. Bhandari, F. Kraher, and T. Poskitt, "Unlimited sampling from theory to practice: Fourier-Prony recovery and prototype ADC," *IEEE Trans. Signal Process.*, vol. 70, pp. 1131–1141, 2021.
- [46] M. Beckmann, F. Kraher, and A. Bhandari, "HDR tomography via modulo Radon transform," in *Proc. IEEE Int. Conf. Image Process.*, 2020, pp. 3025–3029.
- [47] D. Florescu, F. Kraher, and A. Bhandari, "Unlimited sampling with hysteresis," in *Proc. Asilomar Conf. Signals, Syst., Comput.*, 2021, pp. 831–835.
- [48] D. Florescu, F. Kraher, and A. Bhandari, "The surprising benefits of hysteresis in unlimited sampling: Theory, algorithms and experiments," *IEEE Trans. Signal Process.*, vol. 70, pp. 616–630, 2022.
- [49] D. Florescu and A. Bhandari, "Time encoding via unlimited sampling: Theory, algorithms and hardware validation," *IEEE Trans. Signal Process.*, vol. 70, pp. 4912–4924, 2022.
- [50] D. Florescu and A. Bhandari, "Modulo event-driven sampling: System identification and hardware experiments," in *Proc. IEEE Int. Conf. Acoust., Speech Signal Process.*, 2022, pp. 5747–5751.
- [51] M. A. Davenport, Y. Plan, E. Van Den Berg, and M. Wootters, "1-bit matrix completion," *Inf. Inference J. IMA*, vol. 3, no. 3, pp. 189–223, 2014.
- [52] A. Zymnis, S. Boyd, and E. Candes, "Compressed sensing with quantized measurements," *IEEE Signal Process. Lett.*, vol. 17, no. 2, pp. 149–152, Feb. 2010.

- [53] T. Strohmer and R. Vershynin, "A randomized Kaczmarz algorithm with exponential convergence," *J. Fourier Anal. Appl.*, vol. 15, no. 2, pp. 262–278, 2009.
- [54] D. Leventhal and A. S. Lewis, "Randomized methods for linear constraints: Convergence rates and conditioning," *Math. Oper. Res.*, vol. 35, no. 3, pp. 641–654, 2010.
- [55] O. Graf, A. Bhandari, and F. Krahmer, "One-bit unlimited sampling," in *Proc. IEEE Int. Conf. Acoust., Speech Signal Process.*, 2019, pp. 5102–5106.
- [56] P. Debevec and J. Malik, "Recovering high dynamic range radiance maps from photographs," in *Proc. ACM Annu. Conf. Comput. Graph. Interactive Techn.*, 1997, pp. 369–378.
- [57] A. Bhandari and F. Krahmer, "HDR imaging from quantization noise," in *Proc. IEEE Int. Conf. Image Process.*, 2020, pp. 101–105.
- [58] A. Eamaz, F. Yeganegi, and M. Soltanalian, "HDR imaging with one-bit quantization," 2023, *arXiv:2309.03982*.
- [59] T. Feuillen, M. Alae-Kerahroodi, A. Bhandari, and B. Ottersten, "Unlimited sampling for FMCW radars: A proof of concept," in *Proc. IEEE Radar Conf.*, 2022, pp. 1–5.
- [60] M. Wagdy, "Effect of various dither forms on quantization errors of ideal A/D converters," *IEEE Trans. Instrum. Meas.*, vol. 38, no. 4, pp. 850–855, Aug. 1989.
- [61] P. Carbone, "Quantitative criteria for the design of dither-based quantizing systems," *IEEE Trans. Instrum. Meas.*, vol. 46, no. 3, pp. 656–659, Jun. 1997.
- [62] P. Carbone and D. Petri, "Effect of additive dither on the resolution of ideal quantizers," *IEEE Trans. Instrum. Meas.*, vol. 43, no. 3, pp. 389–396, Jun. 1994.
- [63] S. Venkatakrishnan, C. Bouman, and B. Wohlberg, "Plug-and-play priors for model based reconstruction," in *Proc. Global Conf. Signal Inf. Process.*, 2013, pp. 945–948.
- [64] S. Chan, X. Wang, and O. Elgendy, "Plug-and-Play ADMM for image restoration: Fixed-point convergence and applications," *IEEE Trans. Comput. Imag.*, vol. 3, no. 1, pp. 84–98, Mar. 2017.
- [65] S. Boyd, S. P. Boyd, and L. Vandenberghe, *Convex Optimization*. Cambridge, U.K.: Cambridge Univ. Press, 2004.
- [66] S. J. Zahabi, M. M. Naghsh, M. Modarres-Hashemi, and J. Li, "One-bit compressive radar sensing in the presence of clutter," *IEEE Trans. Aerosp. Electron. Syst.*, vol. 56, no. 1, pp. 167–185, Feb. 2020.
- [67] K. Knudson, R. Saab, and R. Ward, "One-bit compressive sensing with norm estimation," *IEEE Trans. Inf. Theory*, vol. 62, no. 5, pp. 2748–2758, May 2016.
- [68] H. Zhu, X. Shang, and J. Li, "Target parameter estimation via one-bit PMCW radar," in *Proc. IEEE Int. Conf. Acoust., Speech Signal Process.*, 2020, pp. 9145–9149.
- [69] J. A. Hogan and J. D. Lakey, *Duration and Bandwidth Limiting: Prolate Functions, Sampling, and Applications*. New York, NY, USA: Springer-Verlag, 2012.
- [70] A. Ma, D. Needell, and A. Ramdas, "Convergence properties of the randomized extended Gauss–Seidel and Kaczmarz methods," *SIAM J. Matrix Anal. Appl.*, vol. 36, no. 4, pp. 1590–1604, 2015.
- [71] B. Polyak, "Gradient methods for solving equations and inequalities," *USSR Comput. Math. Math. Phys.*, vol. 4, no. 6, pp. 17–32, 1964.
- [72] A. Edelman, "On the distribution of a scaled condition number," *Math. Comput.*, vol. 58, no. 197, pp. 185–190, 1992.
- [73] C. Van Loan and G. Golub, *Matrix Computations*. Baltimore, MD, USA: The Johns Hopkins Univ. Press, 1996.
- [74] R. Vershynin, *High-Dimensional Probability: An Introduction With Applications in Data Science*, vol. 47. Cambridge, U.K.: Cambridge Univ. Press, 2018.
- [75] L. Jacques, J. Laska, P. Boufounos, and R. Baraniuk, "Robust 1-bit compressive sensing via binary stable embeddings of sparse vectors," *IEEE Trans. Inf. Theory*, vol. 59, no. 4, pp. 2082–2102, Apr. 2013.
- [76] A. Eamaz, F. Yeganegi, D. Needell, and M. Soltanalian, "Harnessing the power of sample abundance: Theoretical guarantees and algorithms for accelerated one-bit sensing," 2023, *arXiv:2308.00695*.
- [77] S. Foucart and R. G. Lynch, "Recovering low-rank matrices from binary measurements," *Inverse Problems Imag.*, vol. 13, no. 4, pp. 5–10, 2019.
- [78] R. Tibshirani, "Regression shrinkage and selection via the LASSO," *J. Roy. Statist. Soc. Ser. B (Methodological)*, vol. 58, no. 1, pp. 267–288, 1996.
- [79] J. Fan and R. Li, "Variable selection via nonconcave penalized likelihood and its oracle properties," *J. Am. Stat. Assoc.*, vol. 96, no. 456, pp. 1348–1360, 2001.
- [80] H. Zou, "The adaptive LASSO and its oracle properties," *J. Am. Stat. Assoc.*, vol. 101, no. 476, pp. 1418–1429, 2006.
- [81] I. Selesnick, "Sparse regularization via convex analysis," *IEEE Trans. Signal Process.*, vol. 65, no. 17, pp. 4481–4494, Sep. 2017.
- [82] S. Boyd, N. Parikh, and E. Chu, *Distributed Optimization and Statistical Learning via the Alternating Direction Method of Multipliers*. Boston, MA, USA: Now, 2011.
- [83] J. A. Cadzow, "Signal enhancement—A composite property mapping algorithm," *IEEE Trans. Acoust., Speech, Signal Process.*, vol. 36, no. 1, pp. 49–62, 1988.
- [84] S. Rudresh and C. S. Seelamantula, "Finite-rate-of-innovation-sampling-based super-resolution radar imaging," *IEEE Trans. Signal Process.*, vol. 65, no. 19, pp. 5021–5033, Oct. 2017.



Ariam Eamaz (Graduate Student Member, IEEE) received the B.Sc. degree in electrical and computer engineering from the Amirkabir University of Technology, Tehran, Iran, in 2019, and the M.S. degree in the applied mathematics and statistics from the University of Illinois Chicago, in 2023. He is currently working toward the Ph.D. degree in electrical and computer engineering with the University of Illinois Chicago, Chicago, IL, USA. His research interests include mathematical signal processing, statistics, optimization theory, quantization, and randomized algorithms. He is a Member of American Statistical Association-ASA and IEEE Information Theory Society. He was the recipient of the 2019 Best B.Sc. Thesis Award and the Prestigious 2021 Wexler Award.

Kumar Vijay Mishra (Senior Member, IEEE) is with the United States DEVCOM Army Research Laboratory, Adelphi, MD, USA.



Farhang Yeganegi received the B.Sc. degree in electrical and computer engineering from the Amirkabir University of Technology, Tehran, Iran, in 2019. He is currently working toward the Ph.D. degree in electrical and computer engineering with the University of Illinois Chicago, Chicago, IL, USA. His research interests include optimization theory, statistics, numerical linear algebra, and statistical signal processing. He was the recipient of the 2019 Best B.Sc. Thesis Award.



Mojtaba Soltanalian (Senior Member, IEEE) received the Ph.D. degree in electrical engineering (with specialization in signal processing) from the Department of Information Technology, Uppsala University, Sweden, in 2014. He is currently with the Faculty of the Electrical and Computer Engineering Department, University of Illinois at Chicago (UIC), Chicago, IL, USA. Before joining UIC, he held research positions with the Interdisciplinary Centre for Security, Reliability and Trust (SnT, University of Luxembourg), and California Institute of Technology, Pasadena, CA, USA. His research interests include interplay of signal processing, learning and optimization theory, and specifically different ways the optimization theory can facilitate a better processing and design of signals for collecting information, communication, and also to form a more profound understanding of data, whether it is in everyday applications or in large-scale, complex scenarios. He serves as an Associate Editor for IEEE TRANSACTIONS ON SIGNAL PROCESSING and as the Chair of the IEEE Signal Processing Society Chapter in Chicago. He was the recipient of the 2017 IEEE Signal Processing Society Young Author Best Paper Award, and also the 2018 European Signal Processing Association Best Ph.D. Award.